HYDROTHERMALLY GROWN ZINC OXIDE NANOWIRES AND THEIR UTILIZATION IN LIGHT EMITTING DIODES AND PHOTODETECTORS

A THESIS SUBMITTED TO
THE GRADUATE SCHOOL OF NATURAL AND APPLIED SCIENCES
OF
MIDDLE EAST TECHNICAL UNIVERSITY

BY

ELİF SELEN ATEŞ

IN PARTIAL FULFILLMENT OF THE REQUIREMENTS
FOR
THE DEGREE OF MASTER OF SCIENCE
IN
METALLURGICAL AND MATERIALS ENGINEERING

JUNE 2012

Approval of the thesis:

HYDROTHERMALLY GROWN ZINC OXIDE NANOWIRES AND THEIR UTILIZATION IN LIGHT EMITTING DIODES AND PHOTODETECTORS

submitted by **ELİF SELEN ATEŞ** in partial fulfillment of the requirements for the degree of **Master of Science in Metallurgical and Materials Engineering Department, Middle East Technical University** by,

Prof. Dr. Canan ÖZGEN _____
Dean, Graduate School of **Natural and Applied Sciences**

Prof. Dr. C. Hakan GÜR _____
Head of Department, **Metallurgical and Materials Engineering**

Assist. Prof. Dr. Hüsnü Emrah ÜNALAN _____
Supervisor, **Metallurgical and Materials Eng. Dept., METU**

Examining Committee Members:

Prof. Dr. Tayfur ÖZTÜRK _____
Department of Metallurgical and Materials Engineering, METU

Assist. Prof. Dr. Hüsnü Emrah ÜNALAN _____
Department of Metallurgical and Materials Engineering, METU

Prof. Dr. Raşit TURAN _____
Department of Physics, METU

Assoc. Prof. Dr. Caner DURUCAN _____
Department of Metallurgical and Materials Engineering, METU

Assoc. Prof. Dr. Ali ÇIRPAN _____
Department of Chemistry, METU

Date: *15.06.2012*

I hereby declare that all information in this document has been obtained and presented in accordance with academic rules and ethical conduct. I also declare that, as required by these rules and conduct, I have fully cited and referenced all material and results that are not original to this work.

Name, Last name : Elif Selen ATEŞ
Signature :

ABSTRACT

HYDROTHERMALLY GROWN ZINC OXIDE NANOWIRES AND THEIR UTILIZATION IN LIGHT EMITTING DIODES AND PHOTODETECTORS

ATEŞ, Elif Selen

M. Sc., Department of Metallurgical and Materials Engineering

Supervisor: Assist. Prof. Dr. Hüsnü Emrah ÜNALAN

June 2012, 75 pages

Zinc oxide, with its direct wide bandgap and high exciton binding energy, is a promising material for optoelectronic devices. Quantum confinement effect and high surface to volume ratio of the nanowires imparts unique properties to them and makes them appealing for researchers. So far, zinc oxide nanowires have been used to fabricate various optoelectronic devices such as light emitting diodes, solar cells, sensors and photodetectors. To fabricate those optoelectronic devices, many different synthesis methods such as metal organic chemical vapor deposition, chemical vapor deposition, pulsed laser deposition, electrodeposition and hydrothermal method have been explored. Among them, hydrothermal method is the most feasible one in terms of simplicity and low cost.

In this thesis, hydrothermal method was chosen to synthesize zinc oxide nanowires. Synthesized zinc oxide nanowires were then used as electrically active components in light emitting diodes and ultraviolet photodetectors. Hybrid light emitting diodes, composed of inorganic/organic hybrids are appealing due to their flexibility, lightweight nature and low cost production methods. Beside the zinc oxide nanowires, complementary poly [2- methoxy -5- (2- ethylhexyloxy) - 1,4 - phenylenevinylene] MEH-PPV and poly (9,9-di-n-octylfluorenyl-2,7-diyl) (PFO) hole conducting polymers were used to fabricate hybrid light emitting diodes in this work. Optoelectronic properties of the fabricated light emitting diodes were investigated. Zinc oxide emits light within a wide range in the visible region due to its near band edge and deep level emissions. Utilizing this property, violet-white light emitting diodes were fabricated and characterized.

Moreover, to take advantage over the responsivity of zinc oxide to ultraviolet light, ultraviolet photodetectors utilizing hydrothermally grown zinc oxide nanowires were fabricated. Single walled carbon nanotube (SWNT) thin films were used as transparent electrodes for the photodetectors. Optoelectronic properties of the transparent and flexible devices were investigated. A high on-off current ratio around 260000 and low decay time about 16 seconds were obtained. Results obtained in this thesis reveal the great potential of the use of solution grown zinc oxide nanowires in various optoelectronic devices that are flexible and transparent.

Keywords: zinc oxide nanowires, hybrid light emitting diodes, ultraviolet photodetectors

ÖZ

ÇİNKO OKSİT NANOTELLERİN HİDROTERMAL YÖNTEMLE ÜRETİLMESİ VE IŞIK YAYAN DİYOTLARDA VE FOTODEDEKTÖRLERDE KULLANILMASI

ATEŞ, Elif Selen

Yüksek Lisans, Metalurji ve Malzeme Mühendisliği Bölümü

Tez Yöneticisi: Yrd. Doç. Dr. Hüsnü Emrah ÜNALAN

Haziran 2012, 75 sayfa

Doğrudan geniş bant aralığı ve yüksek elektron-hol çifti bağlama enerjisi ile çinko oksit optoelektronik cihaz üretimi için umut vaadetmektedir. Kuantum sınırlaması etkisi ve yüksek yüzey-hacim oranları nanotellere eşsiz özellikler sağlamaktadır ve onları araştırmacılar için cazip hale getirmektedir. Çinko oksit nanoteller şimdiye kadar ışık yayan diyotlar, güneş gözeleri, sensörler, fotodedektörler gibi bir çok optoelektronik cihaz üretiminde kullanılmıştır. Bu optoelektronik cihazları üretmek için metal organik kimyasal buharlaştırma birikimi, kimyasal buharlaştırma birikimi, atımlı lazer birikimi, elektrikli bırakıntı ve hidrotermal gibi yöntemler bulunmuştur. Bu yöntemlerin içinden hidrotermal yöntem basit ve ucuz olması açısından en uygun yöntemlerden biridir.

Bu tez çalışmasında, çinko oksit nanotel üretimi için hidrotermal yöntemi seçilmiştir. Sentezlenen çinko oksit nanoteller ışık yayan diyotlarda ve ultraviyole fotodedektörlerde aktif elektriksel bileşenler olarak kullanılmıştır. Bir inorganik ve bir organik bileşenden oluşan kompozit ışık yayan diyotlar, esnek, hafif ve ucuz yöntemlerle üretilebilirlikleri açılarından dikkat çekmektedirler. Bu çalışmada, kompozit ışık yayan diyot yapısını oluşturmak için çinko oksit nanotellerin yanı sıra, tamamlayıcı poli[2-metoksi-5-(2-etil-heksiloksi)-1,4-fenilen vinil] MEH-PPV and polifloren (PFO) pozitif yarı iletken polimerler kullanılmıştır. Üretilen cihazların optoelektronik özellikleri incelenmiştir. Çinko oksit, enerji bant aralığı ve iç hataları sayesinde görünür dalga boyunda geniş bir alanda ışıma yapar. Bu özellikten faydalanarak eflatunumsu beyaz ışık yayan diyotlar üretilmiş ve karakterize edilmiştir.

Bunun yanısıra, çinko oksitin ultraviyole ışımaya olan duyarlılığından faydalanmak için hidrotermal yöntemle üretilen çinko oksit nanoteller utraviyole fotodedektör üretiminde de kullanılmıştır. Üretilen fotodedektörlerde tek çeperli karbon nanotüp ince filmler transparan elektrot olarak kullanılmıştır. Transparan ve esnek cihazların optoelektronik özellikleri incelenmiştir. Yaklaşık 260000 gibi yüksek bir açma-kapama oranı ve 16 saniye gibi düşük bir akım azalma süresi elde edilmiştir. Bu tezde elde edilen sonuçlar, hidrotermal yöntemle üretilen çinko oksit nanotellerin çeşitli transparan ve esnek optoelektronik cihazlarda kullanılma potensiyelini açığa vurmaktadır.

Anahtar kelimeler: çinko oksit nanoteller, kompozit ışık yayan diyotlar, ultraviyole fotodedektörler

To My Family…

ACKNOWLEDGEMENTS

I would like to thank my advisor Assist. Prof. Dr. Emrah Ünalan for his support and guidance throughout the whole time I have worked on this project and Prof. Dr. Raşit Turan and Prof. Dr. Mehmet Parlak for giving me the opportunity to use almost all the facilities in the Physics Department. I also would like to thank Prof. Dr. Ekmel Özbay, Pakize Demirel, Ayça Emen and Deniz Çalışkan for their help in photoluminescence and electroluminescence measurements. I acknowledge electron microscopy facilities in Metallurgical and Materials Engineering Dept.

I owe my deepest gratitude to my lab-mates and dearest friends, Ayşegül Afal, Barış Özdemir, Burcu Aksoy and Şeyda Küçükyıldız for their infinite support, patience and kindness. I will never forget the awesome time we have had together and I feel very lucky to get to know such great people. I feel the need to single out Mustafa Kulakcı and Şahin Coşkun, for their guidance and patience and never fed up to help me when I' m stuck. I also appreciate the great moral support and positive energies from Sensei Güher Kotan and her angles, Ayşe Merve Genç, Anıl Kantarcıoğlu, Halil İbrahim Yavuz, Evren Tan, Özlem Altıntaş Yıldırım, Furkan Baltaşı, Tuba Cihan Karacaer, Tolga Tokmakci and all my friends in my department who have helped and supported me all along.

I also want to thank my dearest friends Atilla Şahin, Derya Özer, Esra Kadıoğlu, Gül Sarıdoğan, Güneş Uyanıksoy, Mehmet Uysal, Tuba Demirtaş, Özlem Başak İskender and Özge Koçak for being in my life. It's really relieving to have such great friends and know they are always there for me.

And finally, I would like to thank to my whole family, and especially my lovely, precious parents, sisters, grandmother and my darling Murat...I cannot describe my feelings with any words, your love is the most valuable thing I have... Thank you for everything, thank you for always being there for me.

TABLE OF CONTENTS

LIST OF TABLES

TABLES

LIST OF FIGURES

FIGURES

CHAPTER 1

INTRODUCTION

One of the most important issues of this era is the global warming. Causes of the global warming have been under debate for many years. It has been argued that the greenhouse gas emissions are a consequence of burning of fossil fuels, which are the main reasons for global warming. The carbon in these fossil fuels turns into carbon dioxide (CO_2), predominant gas contributing to the greenhouse gas emissions during the burning process. Biggest reason to burn fossil fuels is to generate electricity. To reduce the effect of electricity on global warming, researchers have been looking for renewable energy sources and energy efficient technologies. Solar, wind, geothermal and hydropower systems are some of those sources that produce electricity without CO_2 emission. Beside these renewable energy sources, scientists are also looking for novel materials and methods to reduce energy consumption of the existing technologies. For instance, according to the international energy agency (IEA), one of the biggest portions of the electricity is consumed for lighting, constituting 19%, while promisingly using energy efficient systems could prevent 16 billion tons of carbon footprint over the next 25 years [1]. Today, the most energy efficient lighting method is light emitting diodes (LEDs). Energy savings up to 80% can be achieved by replacing incandescent lamps with LEDs. Moreover, life time of a LED is 25 times longer than that of an incandescent lamp and 3 times longer than that of the compact florescent lamp (CFL). However, commercially available LEDs do have a drawback, which is their high production cost. Commercial LEDs are mostly

produced utilizing gallium nitride (GaN) thin films. GaN is deposited using an intricate and expensive method called metal organic chemical vapor deposition (MOCVD). Moreover, to fabricate GaN LEDs, expensive substrates such as sapphire (Al_2O_3) and silicon carbide (SiC) is used. Therefore, demand for a low cost LED has arisen. Nanomaterials with their unique properties have been attractive for research over the last 3 decades. With lower defect density and low cost production methods such as hydrothermal growth method, zinc oxide (ZnO) nanowires have received great attention. Many groups have reported optoelectronic devices utilizing ZnO NWs such as solar cells [2], sensors [3], photodetectors [4] and light emitting diodes [5]. ZnO is naturally an n-type inorganic semiconductor and obtaining a reproducible and stable p-type ZnO is still under controversy. Main reasons obscuring p-type doping of ZnO are limited solubility of the dopant atoms within the lattice, insufficient charge carrier generation due to deep defect transition levels and difficulty in finding a shallow acceptor material for the wide bandgap of ZnO (3.37 eV) [6,7]. Thus, instead of forming p-n homojunction of ZnO, forming p-n heterojunctions by n-type ZnO with a p-type alternative semiconductor is reasonable for the fabrication of optoelectronic devices. Electroluminescence from n-type ZnO and p-type GaN heterojunctions [8, 9] and n-type ZnO and p-type silicon (Si) heterojunctions [10, 11] have already been reported; however, these type of devices still involve high cost production steps such as MOCVD, chemical vapor deposition (CVD), pulsed laser deposition (PLD). n-type ZnO and p-type Si heterojunctions were produced using simpler and low cost hydrothermal methods also [12, 13]. However, demand for flexible and transparent LEDs inspired the hybrid structures. The hybrid structure includes the combination of a n-type inorganic ZnO with a p-type organic semiconducting materials. Using this new approach cost effective and flexible LEDs were reported [14].

UV radiation is another important issue that affects human life. Various pathologies such as cancer, ageing, Alzheimer`s disease, inflammatory disorders and other ailments are triggered off with the participation of free radical chemical species generated by UV radiation [15, 16]. Importance of UV detection has been increasing

with the increasing size of the ozone hole in Antarctic stratosphere. Nano-scaled UV photodetectors will not only protect human beings from this hazard, but also meet the needs of developing technology. ZnO again will be a good candidate for UV photodetection with its direct wide band gap of 3.37 eV. Many researchers have reported UV photodetectors utilizing ZnO nanowires. However, most of these photodetectors were fabricated using high vacuum and high temperature processes such as CVD, thermal evaporation and sputtering [17-22]. Utilization of hydrothermally grown ZnO nanowires, on the other hand, as the active material in photodetectors would reduce the production cost.

In order to fabricate a truly flexible and transparent UV photodetector, both the active component and the electrodes must be flexible and transparent. SWNT thin films have already been demonstrated as transparent electrodes in optoelectronic devices including solar cells, organic light emitting diodes (OLEDs), electrochromic devices and many others. Therefore, use of single walled carbon nanotube (SWNT) thin films as electrodes will meet these requirements.

In this thesis, ZnO nanowire synthesis methods were discussed and hydrothermally grown ZnO NWs were examined in Chapter 2. Then, in Chapter 3, fabrication of hybrid LEDs utilizing hydrothermally grown ZnO NWs were investigated. Hybrid LEDs were fabricated using different p-type polymers and polymer blends. Among them, successful diode characteristics and electroluminescence was obtained from ZnO and poly{[2- [2′ ,5′ -bis (2″- ethylhexyloxy) phenyl] - 1,4 -phenylenevinylene] – co - [2 – methoxy – 5 - (2′ - ethylhexyloxy) - 1,4 -phenylenevinylene]} (MEH-PPV) heterojunction and ZnO and poly(9,9-di-n-octylfluorenyl-2.7-diyl) (PFO) heterojunction. Structural and optoelectronic properties of these hybrid LEDs were examined in detail. Finally in Chapter 4, development of all solution based UV photodetectors utilizing hydrothermally grown ZnO nanowires and SWNT thin films were examined. Structural, optoelectronic properties of these UV photodetectors fabricated on both glass and flexible polyethylene terephthalate (PET) substrates were investigated in detail.

CHAPTER 2

ZINC OXIDE NANOWIRE SYNTHESIS BY HYDROTHERMAL METHOD

2.1. Introduction

Nanotechnology takes into account the design, fabrication and application of structures whose dimensions, at least in one axis, are in 1 nanometer (nm), a one billionth of a meter (10^{-9} m), to 100 nm range. Working at the nanometer scale dates back more than thousands years. For instance, it's found that gold (Au) nanoparticles were used as an inorganic die to make red color for paintings of ceramic porcelains centuries ago in China [23]. The concepts of nanotechnology emerged from the Richards Feynman's famous talk entitled "There's Plenty of Room at the Bottom" given at Caltech in 1959. Vision of Feynman inspired many scientists and the term nanotechnology was first used by Tokyo Science University Professor Norio Taniguchi in 1974. He defined the term nanotechnology as "the processing of, separation, consolidation and deformation of materials by one atom or by one molecule" [24]. In 1981, K. E. Drexler described a "bottom-up" approach instead of a "top-down approach" that mentioned before by Richards Feynman [25]. The field of nanotechnology gained popularity after that time and still has an increasing trend within the science community.

Materials in nanometer size show remarkably different properties when compared to their bulk form. The main reasons for this are the surface effects and quantum confinement. Nanometer sized structures have large surface to volume ratio. Upon the decrease of the particle size of a structure, ratio of the surface atoms compared to the ones in bulk region increases significantly. Moreover, surface atoms have less number of neighbor atoms and more free (dangling) bonds than the bulk region. These dangling bonds cause the chemical potential at the surface of the materials to be much higher than that in the bulk region. Therefore, overall surface energy increases significantly with decreasing particle size. This dramatic increase in the surface area is one of the reasons for remarkable changes in the properties especially in chemical, thermal and electrical properties of nanomaterials compared to bulk materials [26]. Change in electrical properties of nanomaterials can be attributed to quantum confinement effect. Quantum confinement effect can be explained by the 'particle in a box' model. In bulk materials, Bohr radius (r_B), distance between the electron and hole, is smaller than the size of the bulk crystal and it is free to move all along the lattice. However in nanosized materials, r_B is in the same scale with the diameter of the nanocrystal. This condition leads to the quantum confinement, which causes distinct energy levels instead of continuous energy bands in bulk materials. The gaps between these distinct energy levels are very small; thus, the addition or subtraction of a single atom will cause a change in the bandgap of the nanomaterials and their electrical and optical properties.

Nanostructured materials can be synthesized either by top-down or bottom-up approaches. Top-down approach can basically be described by breaking down the bulk material into nanomaterials; whereas, the bottom-up approach refers to the development of nanostructures with its basic building blocks, atoms. Bottom-up approach is advantageous compared to top-down alternative, because of the absence of surface imperfections. In addition, more homogenous nanostructures with less interior defects and better short or long range ordering can be synthesized by the bottom-up approach [27].

As shown in Figure 2.1, nanostructured materials can be categorized as zero-dimensional (0-D) nanoparticles, one-dimensional (1-D) nanowires, nanotubes and nanorods and two-dimensional (2-D) thin films. The numbers refer to the number of dimensions that are not in nanoscale range [27].

Figure 2.1. Schematic representation of the (a) 0-D, (b) 1-D and (c) 2-D nanomaterials.

2.1.1. Properties of Nanowires

As mentioned above, nanowires are 1-D nanostructures, which mean that they have 2 quantum confined dimensions while leaving one dimension unconfined for electrical conduction. Nanowires with a radius lower than r_B, shows significantly different optical, electrical and magnetic properties from their bulk form due to quantum confinement. Some properties that differ between the nanowires and their bulk forms include high density of electronic states and joint density of states near the energies of their van Hove singularities, enhanced exciton binding energy, diameter-dependent bandgap and increased surface scattering for electrons and phonons [28]. In addition to these, the high surface to volume ratio of nanowires allows the devices to be highly sensitive to the environment leading to fascinating sensing practices. Size, morphology, composition and crystal structure must be comprehended as these parameters control the electrical and optical properties of the devices [29].

Nanowires are also promising for the fabrication of minimized devices with improved performance and lower energy consumption.

2.1.2. Properties of ZnO Nanowires

ZnO is a binary inorganic compound from group II-VI semiconductor. Having a direct wide bandgap and high exciton binding energy (60 meV), that gives the stability against the thermal dissociation of excitons, ZnO nanowires have been promising for optoelectronic devices such as LEDs [5], solar cells [2], sensors [3] and photodetectors [4]. At ambient pressure and temperature, ZnO crystallizes in thermodynamically stable wurtzite form as shown in Figure 2.2, where each O_2^- ion is surrounded by four Zn_2^+ ions at the corners of the tetrahedron, and vice versa.

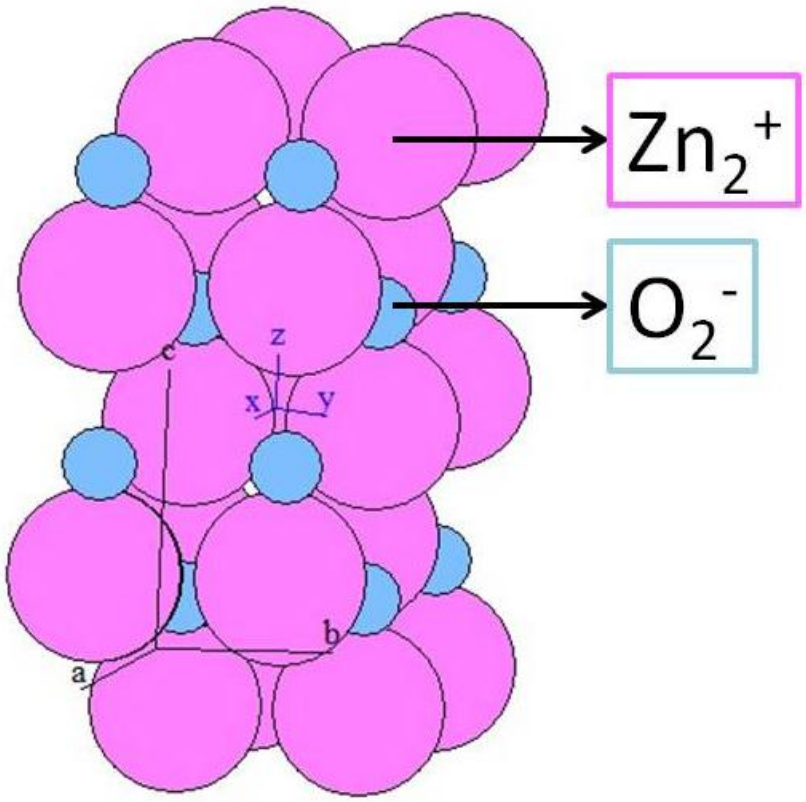

Figure 2.2. Wurtzite crystal structure of ZnO.

This tetrahedral coordination gives rise to a polar symmetry along the hexagonal axis. Number of the properties of ZnO, including its piezoelectricity and spontaneous polarization are caused by this polarity. Moreover, crystal growth, etching and defect generation is induced by this polarization. Typical sp^3 covalent bonding is seen in this tetrahedral system; however, significant ionic character also seen in ZnO, causes the ZnO to stay on the border between the covalent and ionic semiconductor. The polar Zn terminated (000^{-}1) and O terminated (0001) (c-axis oriented), and the non-polar (112^{-}1) faces (a-axis) and (10^{-}10) faces, which both contain an equal number of Zn and O atoms are the four most common face terminations of wurtzite ZnO. Different chemical and physical properties are dominated by the polar faces, whereas the different electronic structure is dominated by the O-terminated face [30].

Due to its wide bandgap, pure ZnO is colorless, which is stunning for transparent electronics. Band edge excitations allow ZnO to emit within UV region. Moreover, ZnO emits light in a wide range within the visible region due to its intrinsic and extrinsic radiative defect levels. ZnO has a number of point defects, which are namely donor defects; zinc interstitials, oxygen vacancies and acceptor defects; zinc vacancies. Growth methods and conditions and growth methods used influence the nature of these defects and thus the emission color. This multi-color emission could be an advantage for optoelectronic applications.

2.1.3. Conventional Zinc Oxide Nanowire Synthesis Methods

ZnO nanowires can be synthesized by various methods. Widely used synthesis methods can be divided into two according to temperature as high temperature (up to 1000 ºC) and low temperature (<100 ºC) methods. Chemical vapor deposition (CVD), metal organic chemical vapor deposition (MOCVD) and pulsed laser deposition (PLD) can be classified as high temperature methods; whereas the electrodeposition and hydrothermal growth methods are classified as low

temperature methods. In this section, most commonly used ZnO nanowire methods will be briefly introduced.

2.1.3.1 *Chemical Vapor Deposition (CVD) Method*

Various nanostructures can be synthesized by CVD method, which rely on vapor liquid solid (VLS) mechanism. The VLS mechanism consists of two steps. At first step, small liquid droplets called catalysts are formed and at the second step nanowires nucleate and grow on these catalyst particles. Transition metal clusters are used as catalysts during the growth of nanowires. The metal can be chosen rationally using the phase diagram on the basis of the solubility of the nanowires' components in the liquid phase. Gold (Au) is generally used as catalyst metal for ZnO nanowire growth due to its ability to form a eutectic mixture with Zn at temperatures far below the melting point of ZnO. The metal droplets are responsible for the determination of the growth direction and diameter of the nanowires.

A schematic of the VLS mechanism of ZnO nanowires is given in Figure 2.3 (a). Typical ZnO nanowire synthesis steps using VLS method can be described as follows: firstly, substrate is covered with Au thin film. Then, the high purity (99.9%) ZnO and graphite powder mixture is prepared and placed in a quartz boat. Carbothermal reduction of ZnO to Zn vapor takes place at elevated temperatures (up to 1000 ºC), Zn vapor then travels towards the cold region of the furnace through the carrying inert gas and then condenses on the Au particles. Precipitation of the oxidized Zn, results in the catalyzed growth of ZnO nanowires (Figure 2.3 (b)). ZnO nanowire formation is influenced by the gas composition in the quartz tube furnace. The thickness of the evaporated Au and the growth time can be tuned to control the diameter and length of the ZnO nanowires, respectively [31].

2.1.3.2 Metal Organic Chemical Vapor Deposition (MOCVD) Method

MOCVD is a chemical vapor deposition (CVD) technique for the epitaxial deposition of semiconducting thin films. Organic compounds, metalorganic or hydride sources that contain the desired element were used as precursors. In case of ZnO, dimethylzinc (DMZ) and diethylzinc (DEZ) are the alternative sources. This technique is also used to grow nanowires over large areas with precise control over growth parameters. Initial cost of a MOCVD system is quite high and therefore this method stands as the most expensive one for the synthesis of ZnO nanowires. Figure 2.3 (c) presents a schematic illustration of a typical MOCVD reactor that is used for the growth of ZnO nanowires. In this case DEZ is used as Zn source and the oxygen (O_2) gas is used as oxygen source. DEZ and O_2 are introduced into the reaction chamber separately and mixed just above the substrate [32]. The substrate temperature may vary between 500 to 1000 ºC and the typical reactor pressure is in the range of 100-400 mbar [33]. A scanning electron microscope (SEM) image of the ZnO nanowires grown using MOCVD is given in Figure 2.3 (d).

2.1.3.3 Pulsed Laser Deposition (PLD) Method

Pulsed laser deposition (PLD) method is widely used for the deposition of high quality thin films. However, in recent years, modified PLD set-ups have been used for the ZnO nanowire growth. A high background pressure of 100 mbars, inert gas usage and building a special deposition set-up with controlled gas flow are some modifications that are necessary for the growth of ZnO nanowires using a PLD system. Temperatures up to 900 ºC are necessary under constant flow of Argon (Ar) gas to grow ZnO nanowires. SEM image of ZnO nanowires grown through PLD method is given in Figure 2.3 (f). Substrate location has an important role in nanowire dimensions. Large diameter and high density nanowires can be synthesized by locating the substrate close to the target due to higher reaction temperature and denser laser plume density as shown in Figure 2.3 (e) [34].

2.1.3.4. Electrodeposition Method

Electrodeposition is a low temperature method that uses electrical current to deposit ZnO nanowires onto a conducting substrate. As shown in Figure 2.3 (g), this method basically consists of a cell system that contains three electrodes; sample as the working electrode, saturated calomel electrode (SCE) as the reference electrode and a metal plate such as platinum (Pt) as the counter electrode all within an electrolytic solution [35]. Generally, electrolyte solution is prepared by zinc nitrate or zinc chloride with precursors like dissolved oxygen (O_2), ammonia (NH_3), calcium chloride ($CaCl_2$) or potassium chloride (KCl). SEM image of the ZnO nanowires grown via electrodeposition is given in Figure 2.3 (h). Applied voltage with the type and concentration of the salt has been used to tune the bandgap, diameter and length of the nanowires [36].

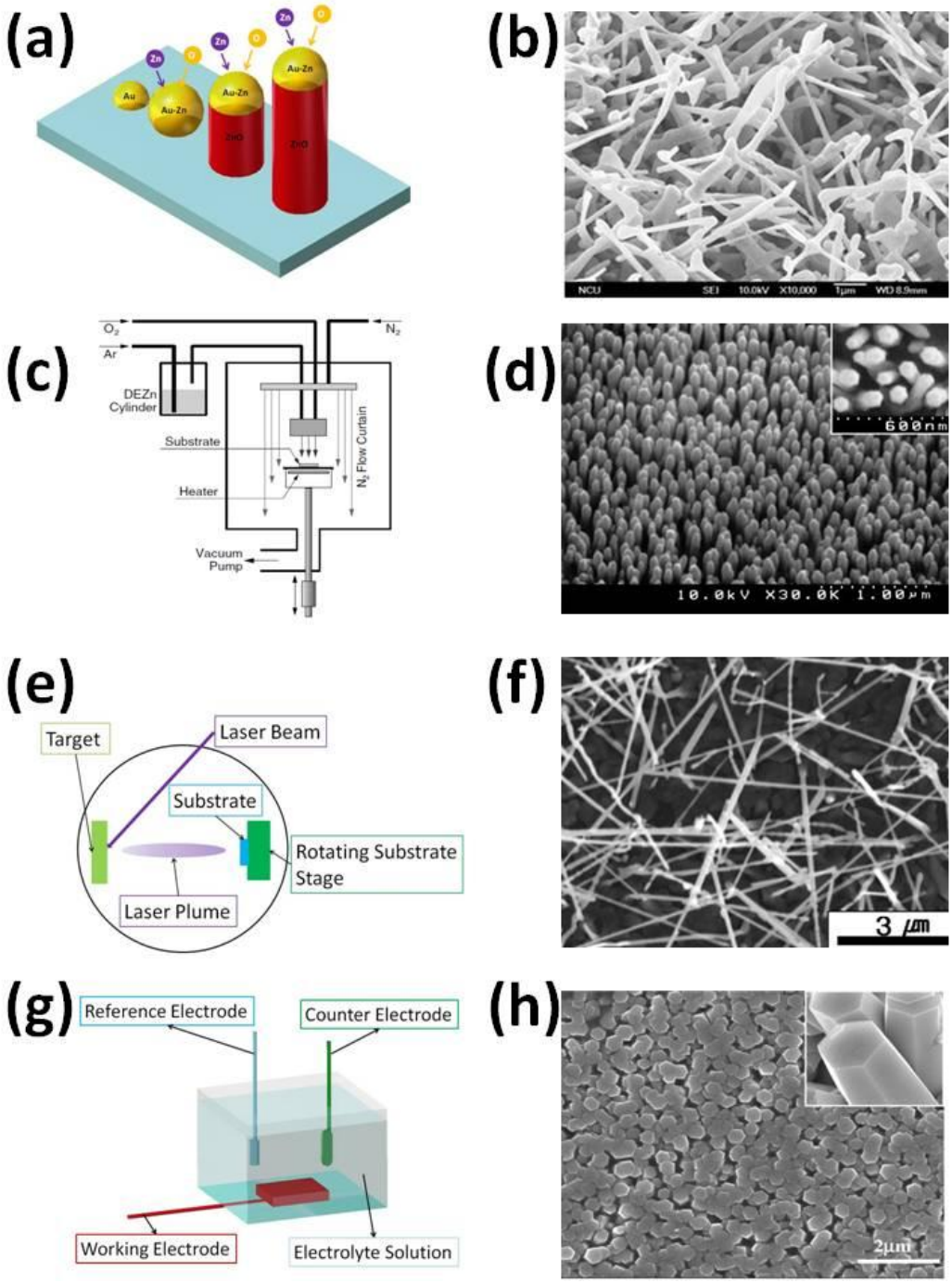

Figure 2.3. Schematic illustration of (a) the stages of VLS growth mechanism, (c) the MOCVD reactor [31], (e) PLD system, (g) electrodeposition system used to grow ZnO nanowires. SEM images of the ZnO nanowires grown using (b) CVD [37], (d) MOCVD [32], (f) PLD [34], (g) electrodeposition [38].

2.1.4. Hydrothermal Method

2.1.4.1. History and Development of Hydrothermal Method

The term "hydrothermal" was first used by Sir Roderick Murchison in the mid 19th century. The first paper on hydrothermal research was on the synthesis of tiny quartz crystals and published in 1845 by K.F.E. Schafthaul. Then, many scientists especially the ones from Europe, started to fabricate other minerals using hydrothermal method. In the beginning, interest in hydrothermal method was only in the fabrication of specific minerals or compounds similar to natural minerals instead of investigating the phase relations or geochemistry of earth' s interior. It was later on realized that using hydrothermal conditions, it is possible to imitate the natural processes that cause the formation of rocks and minerals.

Through the World War II, hydrothermal research facilities became larger and the interest in hydrothermal technology moved to Europe. Today, hydrothermal method is widely used for various purposes by different branches of science including organic chemistry, materials science and biotechnology, and so on [39]. In this thesis, hydrothermal method is used for the growth of ZnO nanowires.

2.1.4.2. Comparison of Hydrothermal Method with the Conventional Methods

Conventional methods like MOCVD, PLD and CVD requires high temperatures and high vacuum levels for the synthesis of ZnO nanowires. Besides, ZnO nanowire synthesis over large areas is not possible using any of these methods in a cost-effective fashion. Hydrothermal method, on the other hand, is a low temperature, almost vacuum-free and therefore a low cost method for the growth of ZnO nanowires. Besides, it is also possible to grow ZnO nanowires over large areas and on various substrates, especially on intriguing ones such as polymers and textiles that

cannot withstand high temperatures. Moreover, high quality nanowires with high yield can be synthesized using environmentally friendly chemicals via hydrothermal method.

In the following part, synthesis of ZnO nanowires using hydrothermal growth method will be reported. Also utilization of ZnO nanowires for development of hybrid LEDs and flexible UV photodetectors will be discussed in detail.

2.2. Experimental Details

2.2.1. Substrate Cleaning

Organic residues on the substrates not only affect the nanowire alignment but also the nanowire quality and their electrical conductivity. To get rid of these organic residues, the first step is to clean the substrates prior to device fabrication. All chemicals were purchased from Sigma-Aldrich and used without further purification. All kind of substrates including soda-lime silica glass, polyethylene terephthalate (PET), indium tin oxide (ITO) coated glass and silicon (Si) wafer were cleaned sequentially with acetone (99.8% pure), isopropanol (99.8% pure) and de-ionized (DI) water in an ultrasonic bath for 10 minutes. Finally, they were dried under nitrogen flow.

2.2.2. Hydrothermal Growth Mechanism of ZnO NWs

Vayssieres et al. first demonstrated the hydrothermal method to synthesize ZnO nanowires on conducting glass and Si substrates back in 2003. This method was further developed by researchers [40].

In this thesis, zinc acetate dihydrate [$Zn(C_2H_3O_2)_2.2H_2O$] and hexamethylene tetramine (HMTA) [$C_6H_{12}N_4$] were used as Zn^{+2} and O_2^- ion sources, respectively. Zinc acetate dihydrate solution in 1-propanol was used for seeding the nanowire growth.

Firstly, to form a seed layer, the substrates were covered with zinc acetate dihydrate solution in 1-propanol by spin coating at 2000 rpm for 1 minute. Then, the substrates were dried on a hot plate at 100 ºC. These processes were repeated depending on the desired nanowire density for devices. Nanowire growth solution was prepared by dissolving equimolar (25 mM) amount of zinc acetate dihydrate and HMTA in DI water (18.3 MΩ). Then, the seed layer covered substrates were submerged into this growth solution kept in a closed bottle. The closed bottle was sealed to prevent the evaporation of water during the growth process. Bottle was then dipped into an oil bath fixed at 90 ºC and growth process took place for the desired amount of time. Schematic illustration of the hydrothermal growth set-up used in this thesis is shown in Figure 2.4. At the end of the growth, substrates were taken off from the solution and washed with DI water to get rid of residual amines and salts and dried under nitrogen flow. A typical top-view and cross-sectional SEM images of the hydrothermally grown ZnO nanowires are shown in Figures 2.5 (a) and (b), respectively.

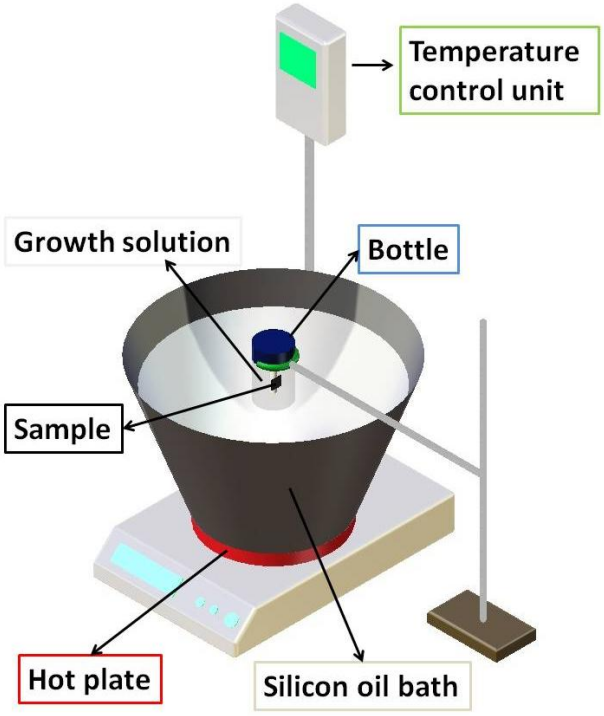

Figure 2.4. Schematic illustration of the hydrothermal growth set-up used in the experiments.

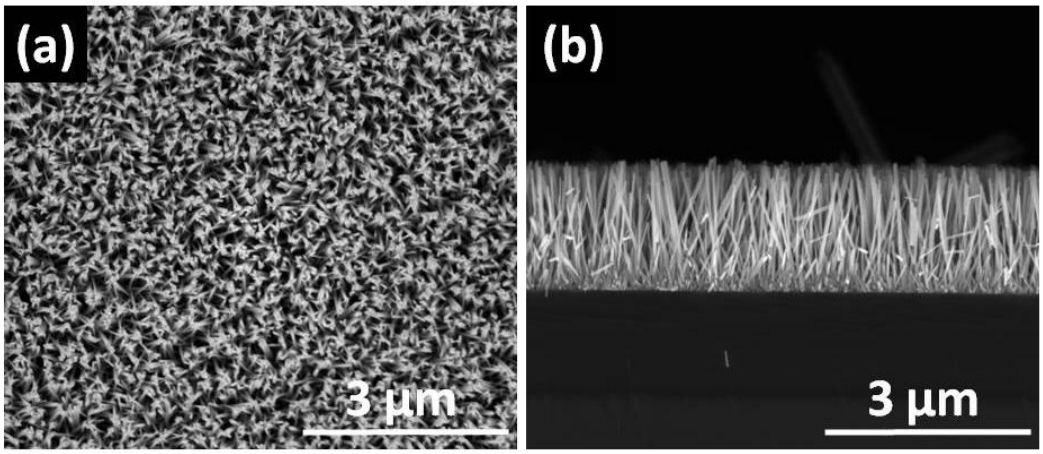

Figure 2.5. (a) Top-view and (b) cross-sectional SEM images of the as-grown ZnO nanowires. Magnifications 40000x.

The following reactions took place during the formation of ZnO nanowires:

$$C_6H_{12}N_4 + 6H_2O \rightarrow 6HCHO + 4NH_3 \quad (1)$$

$$NH_3 + H_2O \rightarrow NH_4^+ + OH^- \quad (2)$$

$$Zn + 2NH_4^+ \rightarrow Zn_2^+ + 2NH_3 + H_2 \quad (3)$$

$$Zn_2^+ + 2\ OH^- \rightarrow Zn(OH)_2 \rightarrow ZnO\ (s) + H_2O \quad (4)$$

At first, HMTA reacts with water and results in ammonia. Then, ammonia reacts with water and dissociates into ammonium and hydroxide ions, which further reacts with zinc ion to form ZnO. Formation of ZnO nanowires is schematically illustrated in Figure 2.6. Firstly, deposition takes place on ZnO seed layer, which has either positively charged Zn or negatively charged O ions. Ions in the seed layer attracts opposite charges from the growth solution. This opposite charge attraction continues until the end of the process or the depletion of the charge sources.

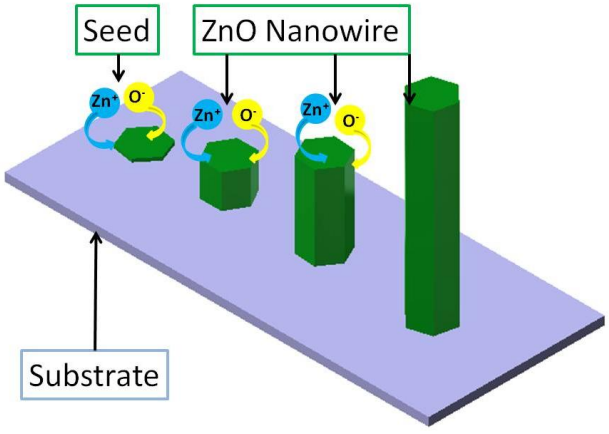

Figure 2.6. Schematic illustration of the ZnO nanowire growth through hydrothermal method.

Nanowire morphology is affected by the growth parameters. Cross-sectional SEM images in Figure 2.7 (a) shows that the length of the ZnO nanowires increases with the growth time. Figure 2.7 (b) shows the change in diameter and length of the ZnO nanowires with respect to time. It can be seen that the length of nanowires increase proportional with time, where the diameter of the nanowires are almost independent of the growth time [41].

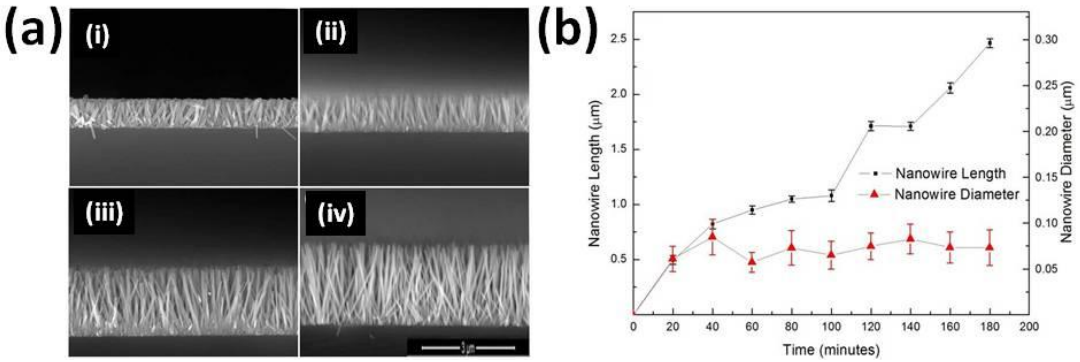

Figure 2.7. (a) Cross-sectional SEM images of the ZnO nanowires that are grown for (i) 40, (ii) 80, (iii) 160 and (iv) 180 minutes. Magnifications are 40000x. (b) Variation of the diameter and length of ZnO nanowires with reaction time [41].

CHAPTER 3

DEVELOPMENT OF LIGHT EMITTING DIODES UTILIZING HYDROTHERMALLY GROWN ZINC OXIDE NANOWIRES

3.1. Introduction

Energy has an important role in our lives and energy consumption is increasing with the development of industry. According to the Stern Review, the earth has warmed by 0.7 ºC since the start of 20th century. Main reason for this warming is thought to be industrialization. Human activities like burning fossil fuels, deforestation and other changes result in an increase in the emission of CO_2 and greenhouse gases like methane and nitrous oxide. Greenhouse gases have a particular effect on global warming. Figure 3.1 shows the "greenhouse effect" that increases the amount of infrared radiation trapped by the atmosphere. Unfortunately, nowadays levels of greenhouse gases reached the highest of all times [42].

Most of these greenhouse gas emissions are caused by the combustion of coal, oil and gas to produce electricity. Energy is consumed for various purposes. Figure 3.2 shows a pie chart of energy consumption in commercial and residential buildings. Lighting is leading with 25% of commercial and 12% of residential energy consumption. According to the International Energy Agency (IEA), the amount of

global consumption of energy for lighting in 2005 was 134.7 petalumen-hours (Plmh) and it has been increasing with the population [1]. However, energy efficient lighting could decrease this energy consumption and thus contribute to the reduction of the greenhouse gas emissions.

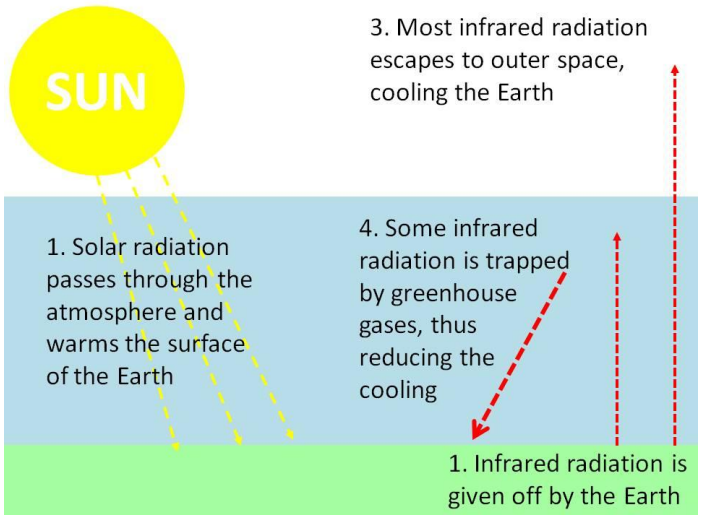

Figure 3.1. Schematic showing of the greenhouse effect [42].

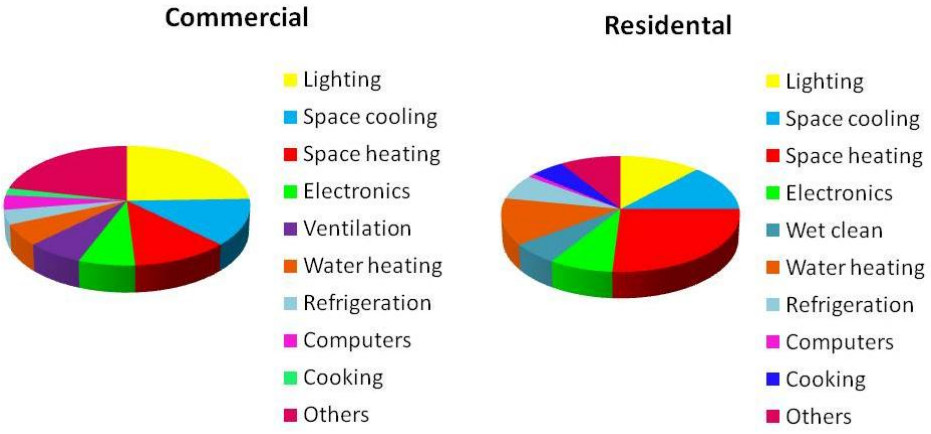

Figure 3.2. Energy consumption by the end user in commercial and residential buildings. [43]

3.1.1. Types of Lighting

3.1.1.1. Incandescent Lamp

In an incandescent lamp, light is produced by the current flow through a tungsten wire. During this process, temperature of the tungsten filament reaches up to 3500 K, which indicates that most of the emission occurs in the infrared region. Luminous efficacy, the ratio of luminous to flux power, of incandescent lamps change in the range between 5-15 lm/W. Beside the low luminous efficacy, short life time (10000 h) and high heat generation are other disadvantages of the incandescent lamps.

3.1.1.2. Tungsten Halogen Lamp

Tungsten halogen lamps are the halogen gas filled version of tungsten lamps. Halogen gas limits the tungsten evaporation and redeposits the evaporated tungsten to the filament. The process temperature is higher compared to the tungsten lamps; therefore, the color of the emitted light is whiter. Luminous efficacy is also higher (12-35 lm/W) than the tungsten lamps. Moreover, their life time is longer (2000-4000 h); but, not long enough to compete with other lamp types.

3.1.1.3. Florescent Lamp

Florescent lamp is a tubular shaped lamp that contains Ar gas and mercury vapor. UV-rays are produced during the current flow by the excitation of electrons in the mercury vapor. UV radiation is converted to white light by the help of a phosphorous coating in the florescent lamp. During that conversion, 65% of the initial photon energy is lost into heat. Luminous efficacy of this type of a lamp is about 100 lm/W and it lasts longer than incandescent and tungsten halogen lamps (10000 - 16000 h). However, it contains poisonous mercury; therefore, should be disposed of properly.

3.1.1.4. Compact Florescent Lamp

Compact florescent lamp (CFL) is the compact form of a florescent lamp. Folding the tubular form into 2 or 6 spirals gives the shape of CFL. Efficacy of CFL is four times higher than the incandescent lamps. Long life time up to 12000 hours is appealing. The use of CFL instead of incandescent lamp will reduce the energy consumption; however, similar to fluorescent lamp its mercury content cannot be disregarded.

3.1.1.5. Light Emitting Diode

Light emitting diodes (LED) are solid-state devices composed of complementary p- and n-type semiconductors. Working principle of a LED is very similar to the semiconductor diodes. LED allows current flow only in one direction. Under forward bias, electrons from n-side and holes from p-side recombine and form an exciton, which release energy in the form of a photon during the transition into a lower energy state. This process is called electroluminescence and illustrated schematically in Figure 3.3. The color of the emitted light depends on the bandgap of the semiconductors that are used to form the p-n junction. Besides the higher luminous efficacy (up to 280 lm/W) [44] and longer life time (up to 50000 hours), mercury-free nature, availability in small size and physical robustness are some advantages of LEDs over other lighting systems.

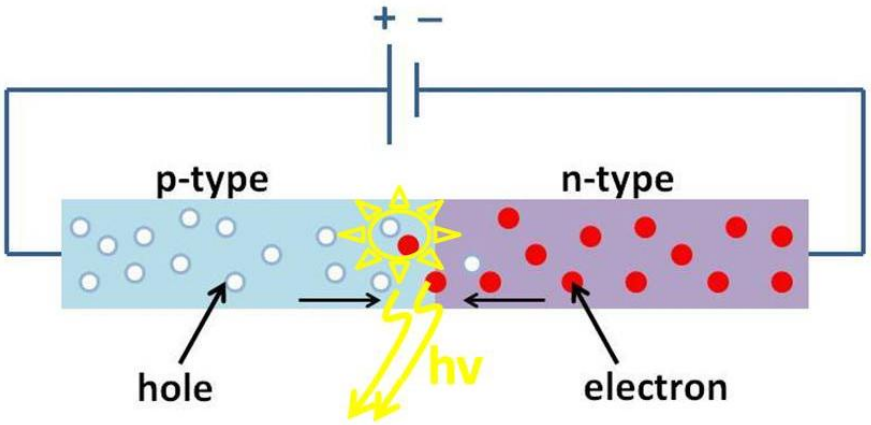

Figure 3.3. Schematic illustration of the electroluminescence process.

3.1.2. History of LEDs

The first LED was reported by Henry Joseph Round during the investigation of unsymmetrical passage of current through a contact of carborundum (SiC) in 1907 [45]. He reported that a yellowish light was observed under an applied bias of 10 V between two points on a SiC crystal and rectifying current-voltage characteristics indicating that the first LED was a Schottky diode. Lossev was then reported a detailed examination of luminescence characteristics of SiC in 1928. Then in 1969, blue light emitting p-n junction devices were fabricated using SiC films [46]. After 1950s, III-V semiconductor compounds became popular in LED research. Gallium arsenide (GaAs) based infrared LEDs were first reported in 1962 [47, 48]. At the same time, visible red LEDs using gallium arsenide phosphide (GaAsP) were also reported [49] and commercialized in 1968 by the Monsanto Corporation [50]. Red, orange, yellow and green LEDs were demonstrated by doping GaAsP with nitrogen (N) [51]. In the late 1960s, James Tietjen came with an idea to develop a flat panel television display. To achieve this idea, he needed full color image displays that contain red, green and blue pixels. At that time red GaAsP and green GaP:N LEDs were already available. To develop blue LEDs, Tietjen and his group member

Maruska synthesized the first gallium nitride (GaN) single-crystal film on sapphire at 850 ºC in 1969. Then, the first blue light emission was reported in 1972 [52].

After the invention of blue LED, white light generation became possible by mixing the three color emission in a way to be perceived as white light. Wavelength converters like phosphors and dyes are other options to generate white light emission. These converters work with the same principle as CFLs. Although these white LEDs offer more efficient and longer life lighting technology compared to its counterparts, higher initial costs due to intricate production methods prevented wide spread use of LEDs. Demand for cheaper LED production gave rise to the investigation of organic light emitting diodes (OLED) [53]. Organic materials generally dissolve in organic solvents. This can be an obstacle during the fabrication of OLEDs that contain more than one organic layer. As a solution of this problem, nowadays, flexible, lightweight and low cost hybrid LEDs, composed of an inorganic and an organic semiconductor layer, became appealing for scientists [35, 54]. In this thesis, hybrid LED structures were fabricated using n-type ZnO nanowires, as inorganic substance, and various p-type polymers or polymer blends, as organic complementary material.

3.1.3. Physics of LEDs

Figure 3.4 (a) shows band diagram of a p-n junction without any applied bias. Conduction band, valance band and Fermi energy levels were indicated as E_C, E_V and E_F, respectively. At this state, free electrons from n-side and free holes from p-side attract each other and recombine at the p-n junction. As a result of this recombination a charge free region called depletion layer form between the p and n sides. Fermi level of n-type and p-type semiconductor were indicated as E_{Fn} and E_{Fp}, respectively, which aligns under zero bias. Donors on the n-side and acceptors on the p-side produce a potential called diffusion voltage (V_D). Under forward bias, electrons and holes are injected into the depletion region and reduce its size, as shown schematically in Figure 3.4 (b). Therefore, the current flow increases and the

charge carriers diffuse into opposite regions and recombine. As a result of this recombination, excitons are formed and they release energy in the form of light upon their decay into a lower energy state. Two recombination mechanisms take place in the semiconductors. First one is the radiative recombination, where the electricity is converted into light by the release of a photon, with an energy equal to the bandgap energy of the semiconductor. The second one is the non-radiative recombination, where the electricity is converted into heat by the vibration of lattice atoms. Non-radiative recombination is caused mainly by the defects in the crystal and not desired in LEDs.

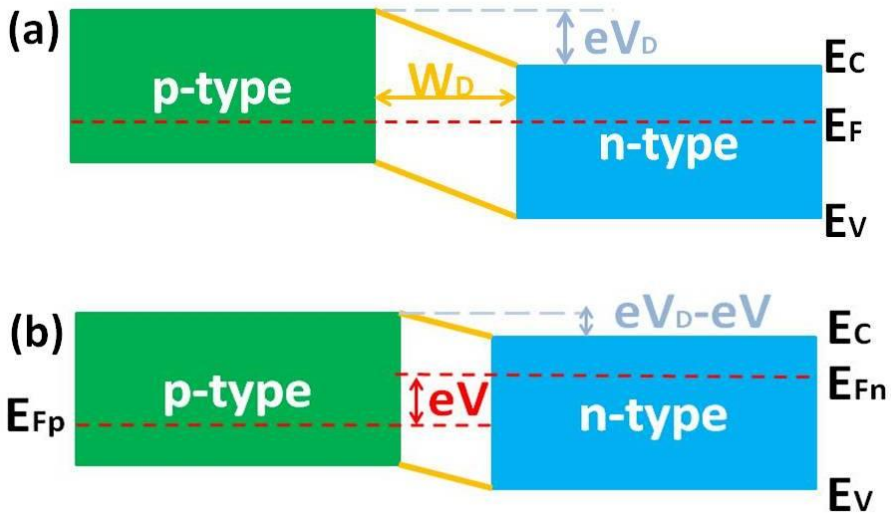

Figure 3.4. Band structure of a p-n junction under (a) zero bias and (b) forward bias.

3.1.4. Hybrid LEDs

As mentioned before, hybrid LEDs consist of organic and inorganic materials. In this thesis, inorganic material was chosen as the n-type ZnO nanowires and the organic part is the p-type polymers or polymer blends. Figure 3.5 shows the two device structures that were examined. Highly conducting p-type polymers were chosen to fabricate these devices. To optimize the hole injection into ZnO, highest occupied

molecular orbital (HOMO) levels of the polymers were chosen to be close to the valance band edge of ZnO. Moreover, lowest unoccupied molecular orbital (LUMO) levels of the polymers must have higher barrier to block electron injection from ZnO to polymers. One of the selected polymers was Poly (3, 4-ethylenedioxythiophene) poly (styrenesulfonate) (PEDOT:PSS, Clevios PH500 and PVPCH800) which is a positively doped highly conducting conjugated polymer. Poly[2-methoxy-5-(2-ethylhexyloxy)-1,4-phenylenevinylene] (MEH-PPV, Sigma Aldrich), poly(9,9-di-n-octylfluorenyl-2,7-diyl) (PFO, Sigma Aldrich), poly(9-vinylcarbazole) (PVK, Sigma Aldrich), Poly(3-hexylthiophene-2,5-diyl) (P3HT, Sigma Aldrich) and 4,4'-Bis(N-carbazolyl)-1,1'-biphenyl (CBP, Sigma Aldrich) were other selected polymers and they were soluble in organic solvents like toluene and chloroform. Among them, MEH-PPV and PFO were light emitting polymers with good hole conductivity.

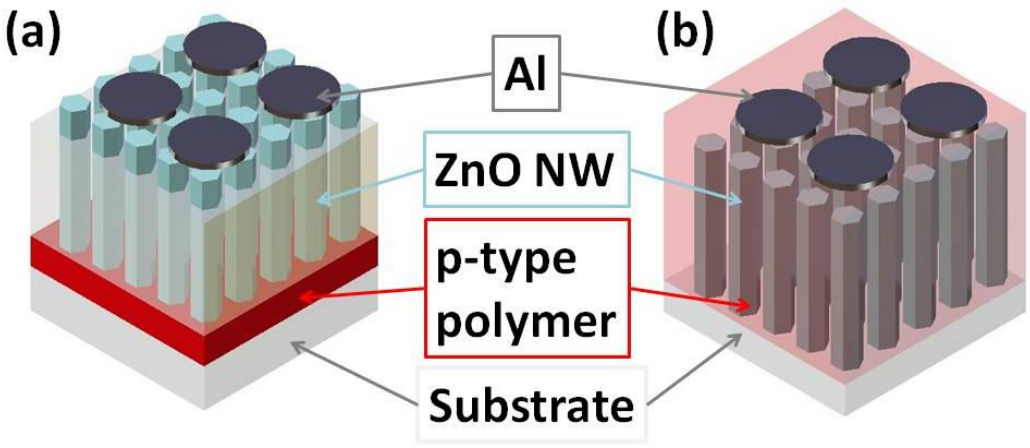

Figure 3.5. Schematic illustration of different hybrid LED structures fabricated in this thesis.

3.2. Experimental Details

Indium doped tin oxide (ITO) coated soda lime glass substrates (Delta technologies, Rs : 4-8 ohms) were used for the fabrication of LEDs. They were first cleaned to get rid of organic residues that can affect the electrical conductivity. Substrates were cleaned according to the procedure mentioned before in the Chapter 2. All chemicals were purchased from Sigma-Aldrich and used without further purification.

As mentioned earlier, two different hybrid LED structures were examined. For the first type that was shown in Figure 3.5 (a), polymers were blended and covered onto the ITO coated glass substrate and ZnO nanowires were grown on these polymer blend layers as described in Chapter 2. Polymer blend solutions were prepared as given in the Table 3.1.

Table 3.1. Solvents and concentrations of the polymer blend solutions.

Polymer Blend	Solvent	Concentration (mg/ml)
MEH-PPV & PVK	Chloroform	3 mg/ml & 6 mg/ml
P3HT & PVK	Chloroform	3 mg/ml & 6 mg/ml
PFO & CBP	Toluene	6 mg/ml & 3 mg/ml

Then, an insulating polymer solution was infiltrated between the ZnO nanowires. Polystyrene (PS, Mw ~ 280,000, Sigma Aldrich) and alternatively AZ5214E (AZ Electronic Materials) positive photoresist was used as insulating polymers. Infiltration parameters were determined for each insulating material by controlled experiments. A 100 nm thick aluminum (Al) top contact was deposited through

evaporation following oxygen plasma etching of the insulating polymer layer on top of the ZnO nanowires.

For the second type of hybrid LED structure that was shown in the Figure 3.5 (b), ZnO nanowires were grown on top of the ITO coated glass substrates as described in Chapter 2. Polymer solutions were prepared as shown in Table 3.2. Then, the polymer solution was spin coated on top of the as-grown ZnO nanowires by spin coating at 1000 rpm. Then, the samples were dried under vacuum at 100 ºC.

Table 3.2. Solvent and concentrations of the polymer solutions.

Polymer	**Solvent**	**Concentration (mg/ml)**
MEH-PPV	Chloroform	5 mg/ml
PFO	Chloroform	5 mg/ml

Finally, a 100 nm thick Al top contact was deposited by a thermal evaporator, as shown in Figure 3.6 (a) through a shadow mask (Figure 3.6 (c)). The components inside the vacuum chamber were shown schematically in Figure 3.6 (b). The evaporator chamber was vacuumed down to a pressure of $1x10^{-6}$ millibars (mbar) then a large current up to 40 A was passed through the resistive tungsten crucible, which generated high temperatures to melt the Al source. Then the Al was evaporated and condensed on top of the substrate. To prevent the current losses that may be caused by the inhomogeneous polymer surface, a shadow mask was used to make array of top contacts instead of a continuous thin film layer. Thickness and radius of the resultant Al contacts in circular geometry was 100 nm and 1.2 mm, respectively. A quartz thickness monitor was used to determine the thickness of the evaporated Al film.

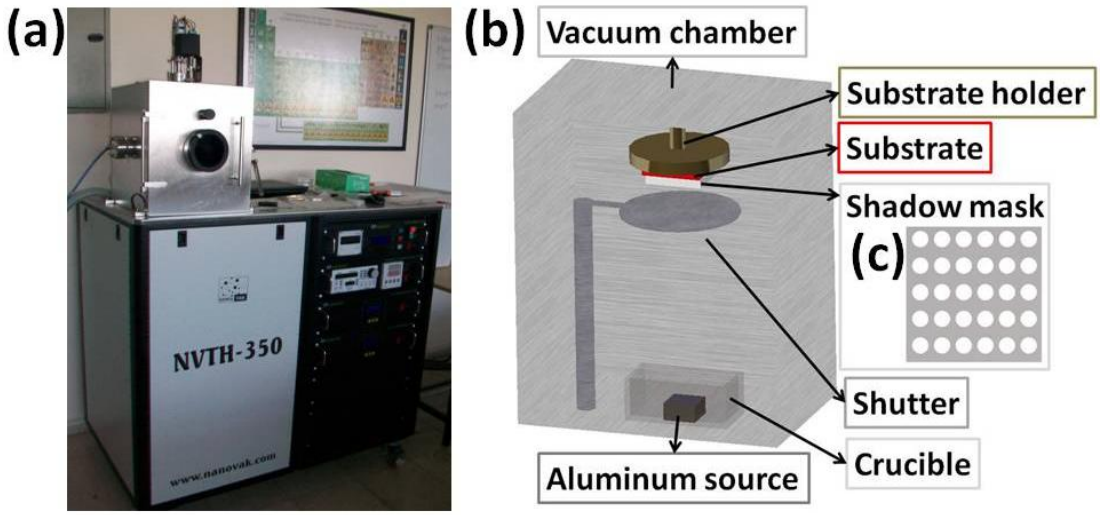

Figure 3.6. (a) Photograph of the thermal evaporator used in the experiments. Schematic illustration of the (b) vacuum chamber components and (c) shadow mask.

3.3. LED Characterization Methods

3.3.1. Scanning Electron Microscope (SEM)

Polymer covered ZnO nanowires were analyzed by SEM (Nova NanoSEM 430) operated at a voltage of 10 kV. In order to obtain cross-sectional images, the samples were cleaved. Both the cleaved edges and the top sides were coated with gold to prevent charging caused by the polymer layer.

3.3.2. Current-Voltage Measurements

Current-voltage measurements have been made using a Keithley 2400 sourcemeter as the voltage source. Voltage was swept between negative to positive values and corresponding current values were recorded using a Labview program.

3.3.3. Photoluminescence Measurements (PL)

During PL measurement, which is a contactless technique, the sample is excited by a laser. As a result of this excitation, material emits light, which is called photo-excitation. The wavelength of the emitted light depends on the energy difference between the excited and ground states of the material. Generally in direct bandgap semiconductors radiative process take place in between the valance and conduction band; therefore, the bandgap of semiconductors can be determined by the photoluminescence technique. Defects in semiconductors are also radiative centers thus; photoluminescence technique can be used to determine specific defect levels. In this thesis, the samples were excited by a continuous laser at 325 nm. Resultant light emissions were collected using a fully integrated Horiba Jobin Yvon spectroscopy system including Triax 550 monochromator and a CCD detector. Schematic of the measurement set-up is shown in Figure 3.7.

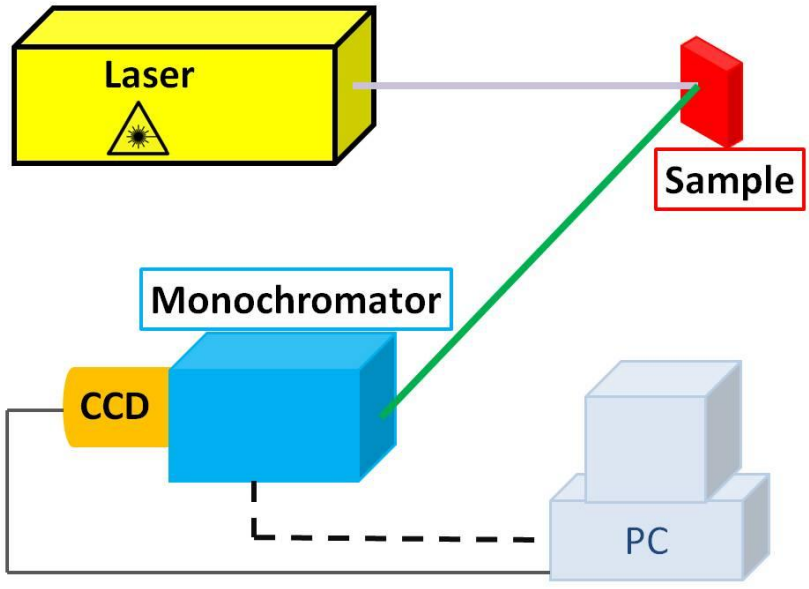

Figure 3.7. Schematic illustration of the photoluminescence measurement set-up.

3.3.4. Electroluminescence Measurements (EL)

EL measurements reveal the wavelength and intensity of the emitted light. During measurements, samples were biased with a Keithley 2400 sourcemeter. Resultant light emissions were collected using a Maya 2000 fiber optic spectrometer.

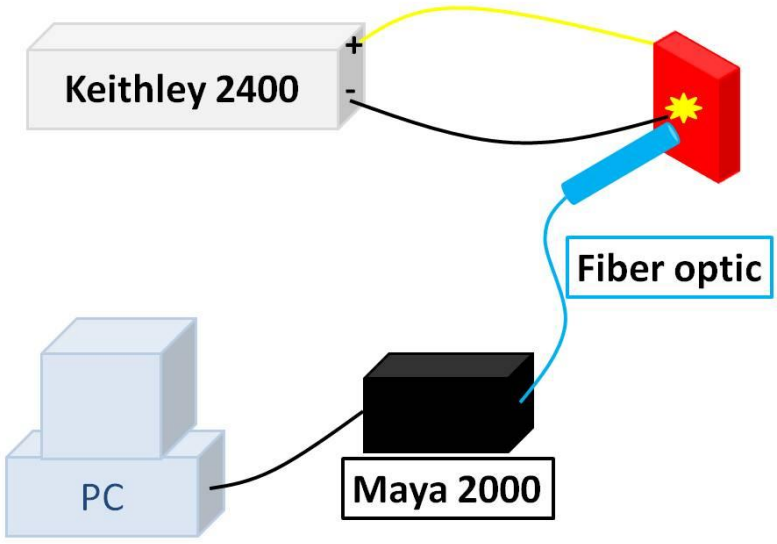

Figure 3.8. Schematic illustration of the electroluminescence measurement set-up.

3.4. Results

3.4.1. ZnO Nanowire and p-type Polymer Hybrid Structure Formation

Cross-sectional and top-view SEM images of the polymer layer covered ZnO nanowires are shown in Figure 3.9 (a) and (b), respectively. The ZnO nanowires

were grown for 30 minutes for this sample and their average length was measured to be 330 nm. From Figure 3.9 (b), it can be clearly seen that the semiconducting polymer solution was filled within the gaps between the nanowires. Therefore, p-n junction was formed not only at the tip of the nanowires but also at the nanowire surfaces, which increases the charge injection efficiency.

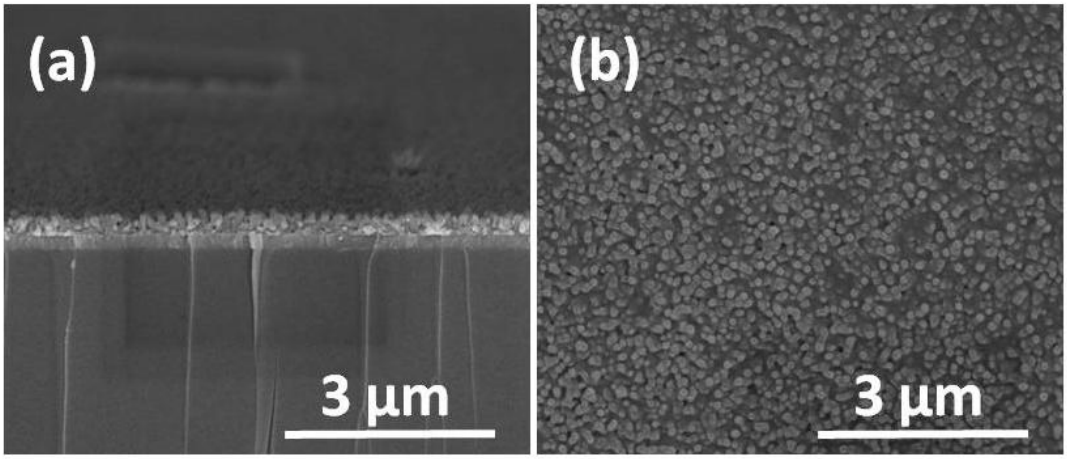

Figure 3.9. (a) Top-view and (b) cross-sectional SEM images of the polymer covered ZnO nanowires.

3.4.2. Optoelectronic Properties of the ITO/ZnO NWs/PFO/Al Hybrid LED

ITO/ZnO NWs/PFO/Al hybrid device and a control sample without the ZnO nanowires were fabricated as explained before. The band diagrams of the two devices are provided in Figure 3.10. In this thesis, ITO was used as anode and Al was used as cathode. Under forward bias, electrons are injected from n-type ZnO nanowires and holes are injected from PFO layer to the ZnO-PFO interface and excitons will be formed and light emission will take place at the interface, which is important for determining color of the emitted light.

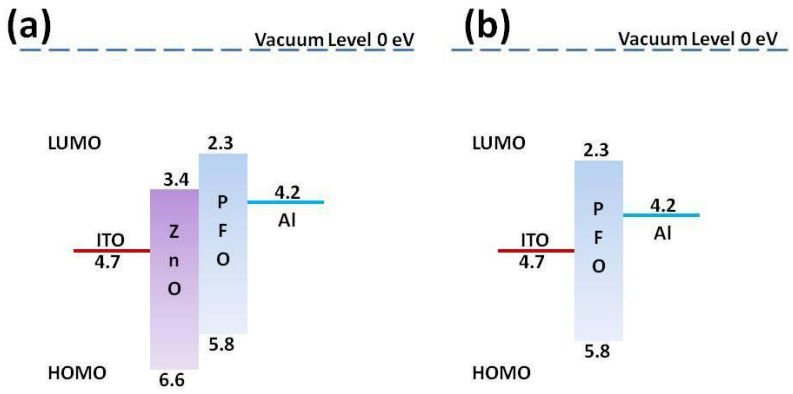

Figure 3.10. Band diagrams of the (a) ITO/ZnO NWs/PFO/Al and (b) ITO/PFO/Al device.

Current-voltage characteristics of the ITO/ZnO NWs/PFO/Al device and the control sample are shown in Figure 3.11 (a) and (b), respectively. From Figure 3.11 (a) it can be clearly seen that the hybrid LED device reveals a rectifying diode behavior; whereas, the device without ZnO nanowires shows ohmic behavior. The diode ideality factor was calculated using thermionic emission theory. According to this theory the current can be described as;

$$\boldsymbol{I = I_S[e^{\left(\frac{V_D}{nV_T}\right)} - 1]} \qquad \textbf{Equation 3.1}$$

, where I is diode current, I_s is saturation current, V_D is diode current, and the n is the ideality factor. V_T is the thermal voltage and is calculated using q/kT equation, where the q is the charge of an electron and k is the Boltzman constant. V_T is approximately 26 mV under normal conditions at room temperature. Ideality factor is calculated using thermionic emission equation and the log plot of the current-voltage characteristics for the hybrid device with nanowires are shown in Figure 3.11 (c). Three distinct regions are indicated on the graph as green, blue and red lines and their ideality factors were calculated to be 4, 15 and 101, respectively. The diode ideality factors were found to be much higher compared to that of an ideal p-n junction diode, where n equals to 1. However, these values are similar to the ones reported in the literature [55]. The reason for this non-ideal behavior was related to

the defect states, such as structural defects, surface contamination, barrier tunneling or generation and recombination within the space charge region in the bandgap of ZnO, which cause additional energy states resulting in multiple current pathways [54, 56]. Defect states in our devices were examined by PL measurements.

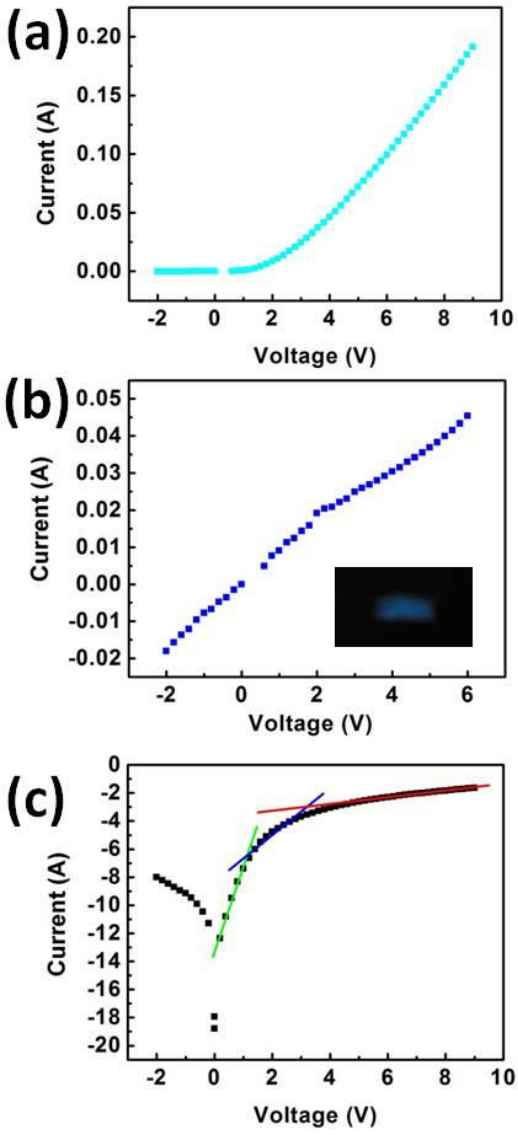

Figure 3.11. Current-voltage characteristics of the (a) ITO/ZnO NWs/PFO/Al and (b) ITO/PFO/Al devices. (c) Logarithmic current-voltage curve of the ITO/ZnO NWs/PFO/Al device. Inset reveals the photograph of the light emission from ITO/ PFO/ Al device.

Room temperature PL characteristics of the PFO layer and ZnO nanowires were first examined individually to distinguish the origin of the peaks in the PL and EL spectra of the final device. PL spectra were taken from the samples fabricated on silicon (Si) substrates and are shown in Figure 3.12 (a) and (b) for ZnO nanowires and PFO, respectively. In order to get rid of noise and make emission peaks recognizable, Gaussian fitting was applied to the PL spectra. Figure 3.12 (a) shows the room temperature Gaussian fit for the PL spectrum of ZnO nanowires. A strong UV emission peak centered around 380 nm, corresponding to the near band emission (NBE) of the ZnO and a broad peak centered on 530 nm, related to the deep level emission (DLE) was observed. Broadness of the DLE band refers to many different deep levels emitting at the same time. The cause of deep level emissions is still under debate [56, 86]. Although it is not specifically clarified, the main reason for deep level emissions has been thought to be intrinsic defects like oxygen vacancy (V_O), zinc vacancy (V_{Zn}), oxygen interstitial (O_i) and zinc interstitial (Zn_i). Green, yellow and red luminescence DLE bands are the ordinary bands encountered in ZnO PL spectra [56]. Green emission band generally attributed to V_{Zn} or V_O; however, it is also claimed that instead of only one of the vacancy type, both the zinc and oxygen vacancies contribute to the emission. Oxygen interstitials are thought to contribute to the yellow and orange band emission and the zinc interstitials are associated with the red emission [56].

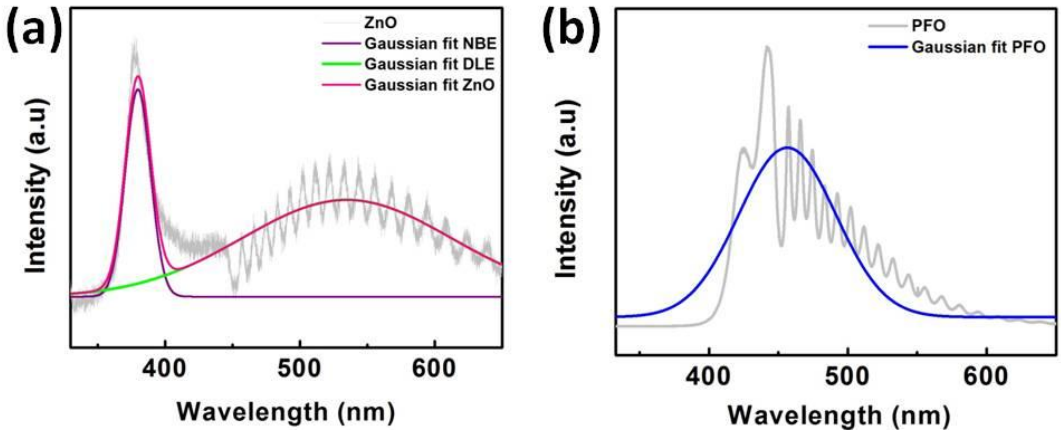

Figure 3.12. PL spectra with Gaussian fit for (a) ZnO nanowires and (b) PFO.

A peak centered around 460 nm which is the main peak of the PFO was observed from the Gaussian fit as shown in Figure 3.12 (b). Excitonic emission and vibronic progression from noninteracting single chains are the origins of this peak [57]. A photograph of the resultant light emission is given in the inset of Figure 3.11 (b).

The PL spectrum and Gaussian fit for the PFO covered ZnO nanowires are shown in Figure 3.13 (a). A UV peak around 430 nm, attributed to NBE of ZnO, a broad band centered at 500 nm, attributed to DLE of ZnO and a blue emission peak at 460 nm, main peak of PFO was observed. The EL spectrum of the ITO/ZnO/PFO/Al device is shown in Figure 3.13 (b). A UV emission peak around 390 nm caused by the NBE emissions of ZnO and a broad peak involving the main emission peak of PFO at 460 nm, the green emission peak centered at 550 nm and the red emission peak centered at 630 nm was observed. A photograph of the resultant light emission is given in the inset of Figure 3.13 (b). The difference between the PL and EL spectra could be caused by the exciplex formation. Exciplex, a transient donor-acceptor complex between the excited state of donor and ground state of acceptor, is formed by two molecules from different materials. Emission of the exciplex occurs by the recombination of electron in LUMO of donor and hole in HOMO of acceptor. Exciplex emissions have higher wavelengths than the excited emissions, thus this can explain the difference between the PL and EL spectrum [58].

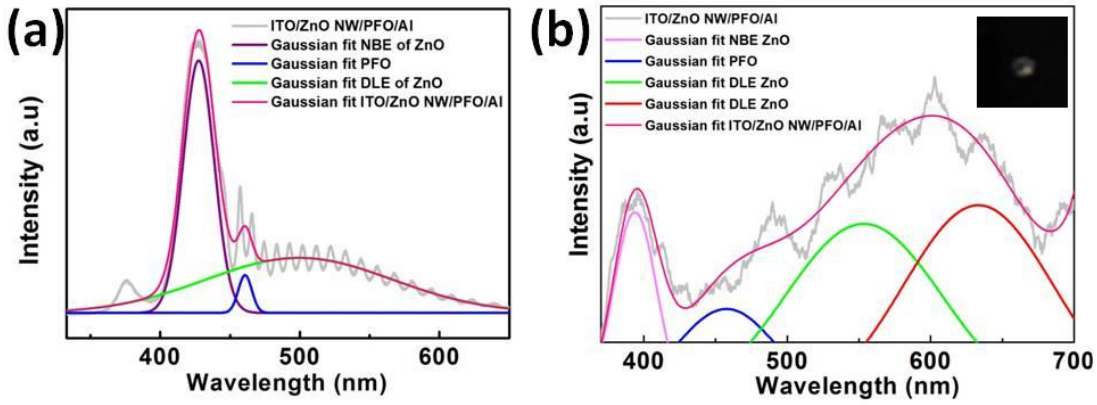

Figure 3.13. (a) PL spectra of the PFO covered ZnO nanowires and (b) EL spectra of the ITO/ZnO NWs/PFO/Al device. Gaussian fits are also provided. Inset reveals the photograph of the light emission from ITO/ZnO NW/ PFO /Al device.

To increase the light emission intensity, different methods were investigated. Firstly, devices were fabricated with different ZnO nanowire lengths. To do this, growth time of the ZnO nanowires were alternated. Then, devices were fabricated with a PFO density of 5 mg/ml. The resultant current-voltage characteristics of the devices are shown in Figure 3.14 (a). It can be clearly seen that reverse current leakage was observed form the devices except the one with 2.5 μm ZnO nanowires. This situation was caused by the imbalanced charge carrier injection from n-side to p-side and vice versa. Alternatively, the PFO solution concentration was alternated and length of the ZnO nanowires was fixed at 2.5 μm. The current-voltage characteristics are shown in Figure 3.14 (b). For those kind of devices, reverse current leakage was observed from the device with a PFO density of 15 mg/ml. No reverse current leakage was observed from the device with a PFO density of 25 mg/ml; but, the threshold voltage of that device was found to be higher than the device with a PFO density of 5 mg/ml. Therefore, no positive device improvement was obtained.

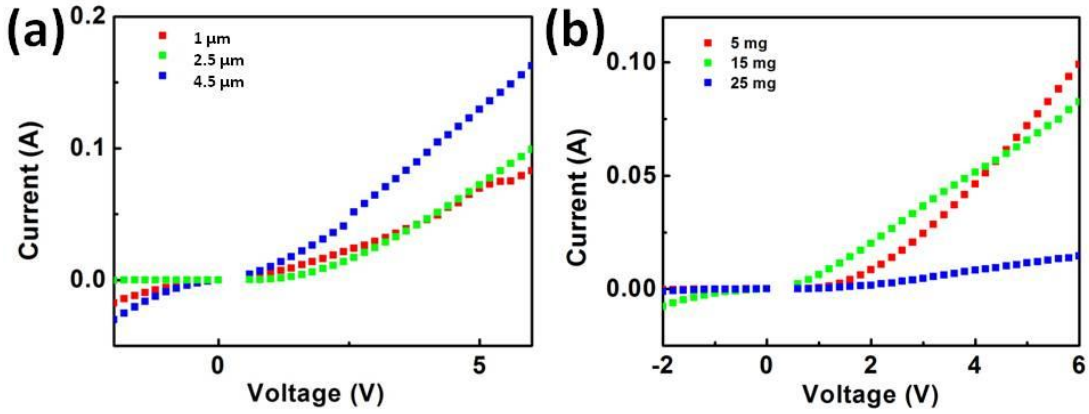

Figure 3.14. Current - voltage characteristics of the ITO/ZnO NWs/PFO/Al devices with (a) different ZnO nanowire lengths and (b) different PFO concentrations.

3.4.3. Optoelectronic Properties of the ITO/ZnO NWs/MEH-PPV/Al Hybrid LEDs

ITO/ZnO NWs/MEH-PPV/Al hybrid device and a control sample without ZnO nanowires were fabricated as explained before. The band diagrams of the two devices are shown in Figure 3.15. Similar to the previous case, ITO was used as anode and Al was used as cathode. Under forward bias, electrons are injected from n-type ZnO nanowires and holes are injected from MEH-PPV layer to the ZnO- MEH-PPV interface and excitons will be formed and light emission will take place at the interface, which effects the color of the emitted light. Moreover, it should cover the ZnO nanowires to avoid the leakage current.

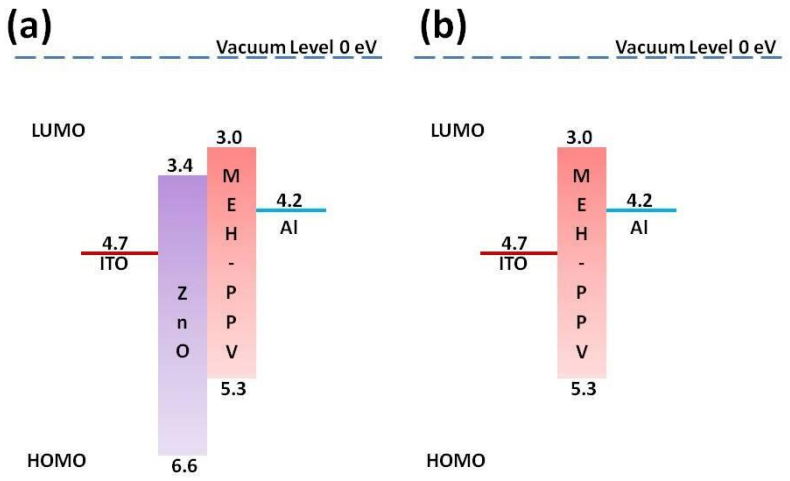

Figure 3.15. Band diagrams of the (a) ITO/ZnO NWs/MEH-PPV/Al and (b) ITO/ MEH-PPV/Al device.

Current-voltage characteristics of the ITO/ZnO NWs/MEH-PPV/Al device with its control sample are shown in Figure 3.16 (a) and (b), respectively. From Figure 3.16 (a) it can be clearly seen that the hybrid LED device shows rectifying diode behavior; whereas, the device without ZnO nanowires shows ohmic behavior. Ideality factor is calculated using thermionic emission equation and the logarithmic plot of current-voltage curve is provided in Figure 3.16 (c).Three distinct regions are indicated on the graph as green, blue and red lines and their ideality factors are calculated to be 5.4, 13 and 41, respectively. The reasons for this non-ideal behavior were explained in detail before in Chapter 3.4.2.

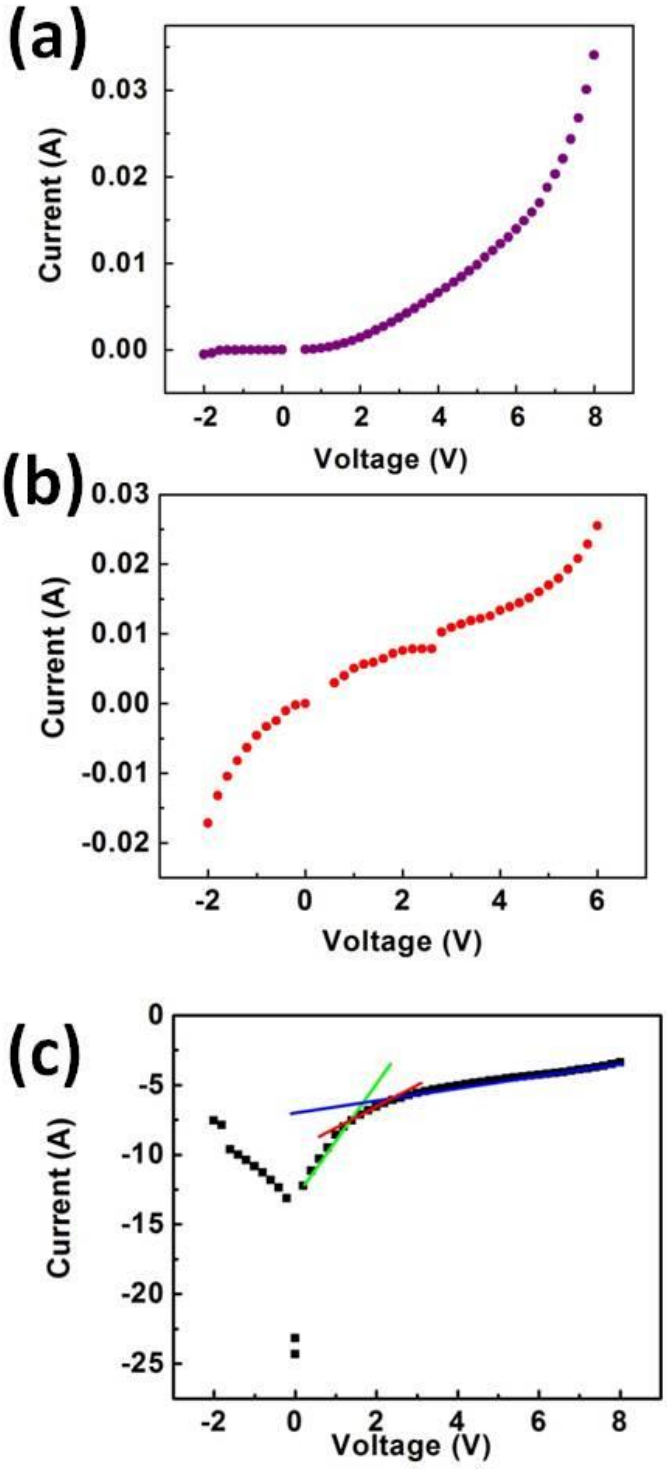

Figure 3.16. Current-voltage characteristics of the (a) ITO/ZnO NWs/MEH-PPV/Al and (b) ITO/MEH-PPV/Al devices. (c) Logarithmic current-voltage curve of the ITO/ZnO NWs/MEH-PPV/Al device.

Room temperature PL and EL characteristics of the MEH-PPV were examined individually. The resultant PL and EL spectra are shown in Figure 3.17 (a) and (b), respectively. Similar to the previous case, Gaussian fits are applied to the PL spectra. Excitonic emission around 580 nm is observed for both PL and EL spectra of MEH-PPV.

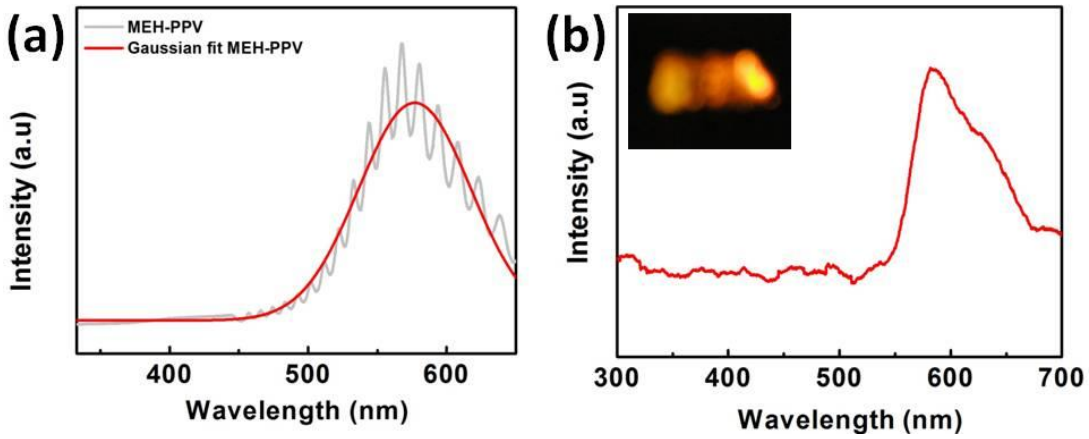

Figure 3.17. (a) PL spectra and (b) EL spectra of MEH-PPV. Gaussian fit is provided for PL spectrum. Inset reveals the photograph of the light emission from ITO/ MEH-PPV /Al device.

The PL spectrum and corresponding Gaussian fit for the MEH-PPV covered ZnO nanowires is shown in Figure 3.18 (a). A strong UV peak around 390 nm, attributed to NBE of ZnO and a broad band centered at 565 nm, attributed to the exciton emission of MEH-PPV and the DLE emissions of ZnO nanowires were observed. The EL spectrum of the ITO/ZnO NWs /MEH-PPV/Al device is shown in Figure 3.18 (b). A strong UV emission peak at around 390 nm caused by the NBE emissions of ZnO and a broad peak involving the exciton emission of MEH-PPV and the DLE emissions of ZnO centered at around 630 nm was observed. The strong UV emission peak in both PL and EL spectra overpowered the other emissions; thus, the color of emitted light. Bright yellowish red light emission observed from the MEH-PPV as

can be seen from the inset of Figure 3.17 (b); where, the color of emitted light shown in the inset of Figure 3.18 (b) turn into violet-white in ZnO NW/MEH-PPV hybrid LED. The little difference between the PL and EL spectra around the visible region could be caused by the exciplex formation as mentioned before.

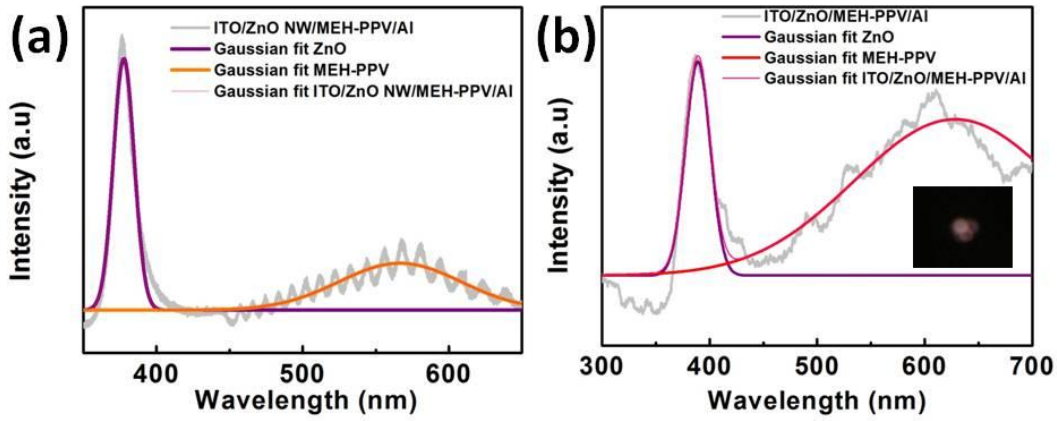

Figure 3.18. (a) PL spectra of the MEH-PPV covered ZnO nanowires and (b) EL spectra of the ITO/ZnO/MEH-PPV/Al device. Gaussian fits are also provided. Inset reveals the photograph of the light emission from ITO/ZnO/ MEH-PPV /Al device.

To increase the intensity of emitted light, devices were fabricated with different ZnO nanowire lengths. The resultant current-voltage characteristics of the devices are shown in Figure 3.19. Threshold voltages of the all three devices were found to be nearly the same. Rectifying behavior of the device with the longest ZnO nanowires was observed to be better than others. However, as a result of these experiments, no significant change was observed in the intensity of emitted light.

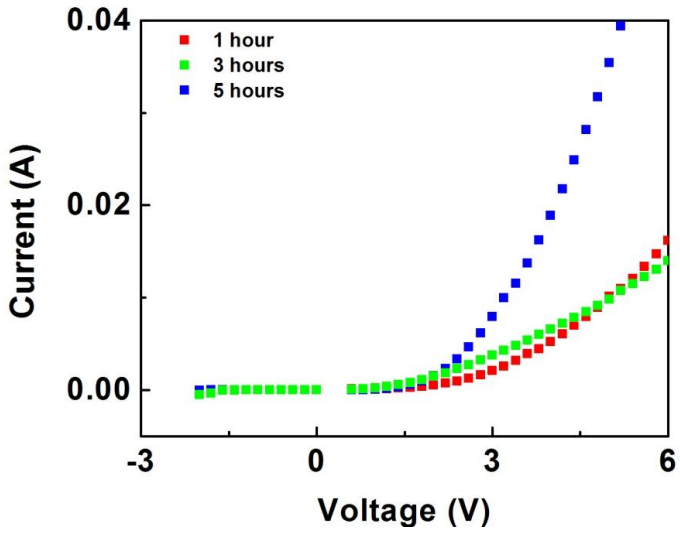

Figure 3.19. Current - voltage characteristics of the ITO/ZnO NW/MEH-PPV/Al device with different ZnO nanowire lengths.

CHAPTER 4

DEVELOPMENT OF ALL SOLUTION BASED UV PHOTODETECTORS UTILIZING HYDROTHERMALLY GROWN ZINC OXIDE NANOWIRES

4.1. Introduction

Nowadays, UV radiation coming from the sun became a danger for human health with the decrease in the thickness of the ozone layer of the stratosphere. UV rays are divided into three parts which are namely UVA, UVB and UVC. As can be seen from the Figure 4.1 UVC has the shortest wavelength among the others and is absorbed by the ozone layer and cannot reach the human body. However, most of the UVB and UVA can reach the skin.

UVB with a shorter wavelength reaches the outer layer of the skin and causes tan by activating melanin production, stimulating the increase in the dark-colored pigment. Moreover, UVB rays cause damage to deoxyribonucleic acid (DNA) and higher doses of UVB induce skin cancer [59]. UVA rays also activate melanin pigments and go further inside the skin, which enhance the skin cancer generation. Moreover, UVA rays change the balance of the immune system and reduce the body's defense against diseases. Eyes also affected negatively from the UV rays, which result in

diseases like eye cancer, cataracts and pterygium [60]. UV detection is one of the most important ways for awareness and protection from harmful sunlight.

Beside the detection of ozone and harmful biological agents and solar radiation, detection of missile exhaust and secure transmission of data in space are other usage areas of UV photodetectors. High response coefficient, linear photocurrent as a function of the incident optical power, high degree of spectral selectivity and for semiconductors large bandgap energy are some of the desired properties for these applications. Depending on the application, needs can be changed [61].

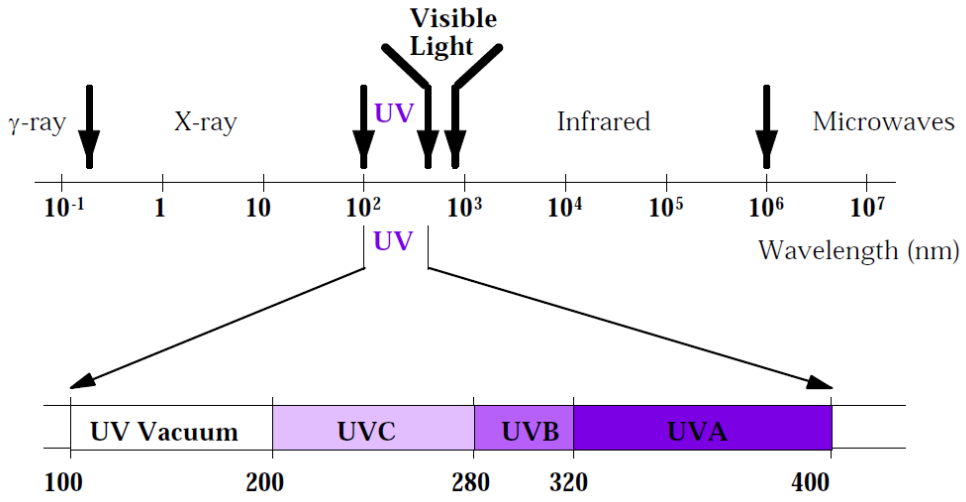

Figure 4.1. UV portion of the electromagnetic spectrum [63].

Photomultiplier tubes have been preferred for detection with their unapproachable sensitivity; however, giant, fragile and expensive structure of these systems cannot satisfy today's demand for small sized electronic devices. Development of UV photodetectors based on semiconductors rear up since they provide unrivaled flexibility, portability and miniaturization.

4.1.1. Fundamental Working Principles of Photodetectors Based on Semiconductors

Photodetection in semiconductors take place by the generation of electron-hole pairs under illumination. During illumination, photons with a higher energy than the bandgap of the semiconductor, excites electrons from valance to conduction band of the semiconductor. A photocurrent is formed due to the traveling of free electrons along the conduction band and moving of holes remained in the valance band under the effect of an electric field. These separated electrons and holes are called photogenerated free charge carriers and the number of these carriers increase leading to an increase in photocurrent with the intensity of the illumination.

4.1.1.1. Photovoltaics

Charge separation in photovoltaic devices becomes possible using the internal electric field at the junction. Schottky barrier photodiodes, metal-semiconductor-metal (MSM) photodiodes, p-n junction, and p-i-n photodetectors are in this class of photodetectors.

4.1.1.2. Photoconductors

For the same material, photoresponse of photoconductors is much greater than the photovoltaic detectors. Photoconductors comprise of a semiconductor layer and two ohmic contacts. Schematic illustration of photoconduction process is shown in Figure 4.2; a constant bias voltage (V_B) is applied at the ohmic contacts that results in a bias current (I_B) flowing through the semiconductor material. The region between the two electrodes called active optical surface, where photogenerated charge carriers are

produced under illumination. New current as a result of these photogenerated charge carriers is called photocurrent (I_{PH}) that increases the total current with the addition of bias current. Thus, the conductivity of the device increases under illumination.

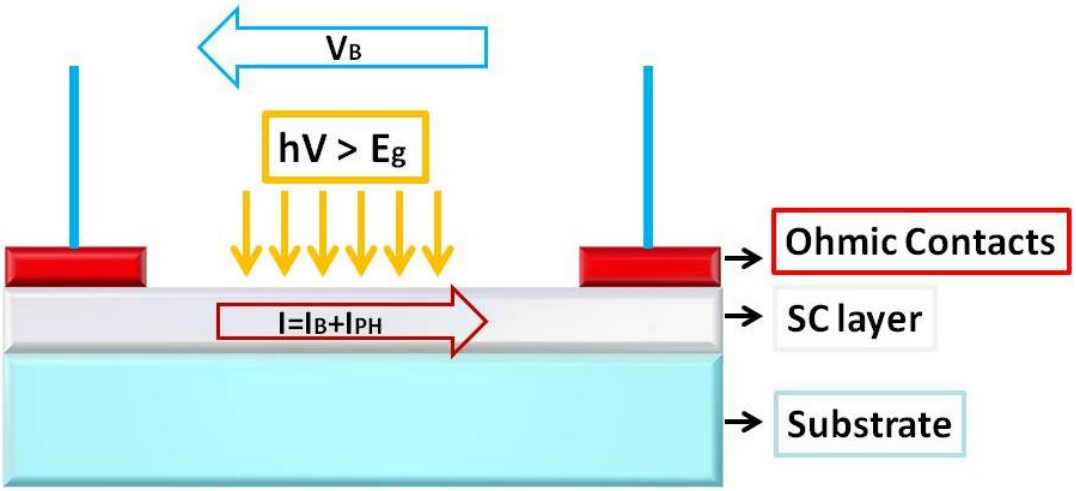

Figure 4.2. Schematic illustration of the photoconductors.

4.1.2. Conventional UV Photodetectors Based on Semiconductors

Usually, Si photodiodes are used for UV photodetection. However, due to the nature of Si, these types of photodetectors have some restrictions. For example, device ageing is one of the most important obstacles of narrow-bandgap Si UV photodetectors as a result of exposure to higher energy photons compared to its bandgap. Sensitivity to low energy radiation is another obstacle, so that filters must be used to detect UV rays only. Moreover, cooling systems are required to reduce the dark current; however, they are known to lower detectivity. Therefore, wide bandgap semiconductors like silicon carbide (SiC), III-nitrides and some II-V compounds are preferred for UV photodetection. The thermal conductivity of these wide bandgap semiconductors are much larger than that of the Si thus, they can be used for high temperature and high power processes. Generally, passivation is not required for

these devices; therefore, they exhibit high responsivity and stability at short wavelengths. Moreover, their radiation hardness is high due to strong chemical bonds [63].

4.1.3. UV Photodetectors Based on ZnO

Among wide bandgap semiconductors, ZnO has been the most promising one due to low cost production methods, its strong radiation hardness, high chemical stability and large bandgap. UV photoresponse in ZnO films were first published in 1954 and research on this area gained acceleration after 1980 [64].

4.1.3.1. UV Photodetectors Based on ZnO Thin Films

Gold (Au), Al, platinum (Pt), and ITO were used as the electrodes of ZnO thin film photodetectors [64]. In an example, ZnO thin film photodetectors that have a photoresponsivity of 400 A/W at an applied bias of 5V with a rise and fall time of 1 and 1.5 μs, respectively, was fabricated using MOCVD on sapphire substrates [65]. In an other example, 100 and 20 ns rise time was obtained from devices fabricated by sputtered ZnO thin films on quartz substrates with Al and Au electrodes [66, 67]. Moreover, using ITO and Al electrodes, rise time of 71.2 ns and a decay time of 377 μs was obtained with a responsivity of 1.616 A/W at 5V [68].

Due to their simple structure, fabrication ease and low capacitance per unit area, MSM photodetectors have also received attention. MOCVD [69], laser assisted molecular beam deposition (LAMBD) [70], radio frequency (RF) magnetron sputtering [71], atomic layer deposition (ALD) [72] and molecular beam epitaxy (MBE) [73] are some of the investigated methods for the fabrication of ZnO based

MSM photodetectors. Response times down to 12 ns and recovery times down to 20 ns and a 1.5 A/W responsivity at 5V were obtained with Ag electrodes [69].

Schottky photodiodes have many advantages like high quantum efficiency, response speed and UV/visible contrast, low dark current and zero-bias operation. Several methods including plasma assisted molecular beam epitaxy were used to fabricate ZnO Schottky photodiodes [64].

Another way to fabricate ZnO thin film photodetectors is the formation of p-n photodiodes. MBE [74] and RF sputtering [75] are some of the utilized methods for the fabrication of this type of photodiodes.

4.1.3.2. UV Photodetectors Based on ZnO Nanowires

Using ZnO nanowires, flexible, transparent and low cost photodetectors can be fabricated. Yang et al was first to demonstrate ZnO nanowire based photodetectors in 2002 [76]. ZnO nanowires were synthesized using a vapor phase transport process. Au electrodes were deposited using electron beam evaporation. The resistivity of the nanowires was found to decrease 4 to 6 orders of magnitude upon UV light exposure. Inspired from this study, ZnO nanowire based UV photodetectors were fabricated using different synthesis methods. Generally high vacuum and high temperature systems like CVD [4, 18], and PLD [77] were used for the growth of ZnO nanowires. Hydrothermal method was also used for the growth of ZnO nanowires [78, 79]. However, fabrication of metal electrodes was realized through high vacuum process like thermal and e-beam evaporation. In fact, fabrication of a fully transparent and flexible device necessitates that both the active element and the electrodes must individually possess these properties. Instead of high vacuum processed metal electrodes, transparent conducting layers like SWNT thin films can be used to meet these requirements.

Using ZnO nanowires instead of ZnO thin films not only enable flexibility but also increase device performance. Su et al. showed that carrier lifetime of ZnO nanowire photosensors are longer and photoresponsivity values of these photosensors are much larger compared to their counterparts fabricated with ZnO thin films [78].

4.1.4. SWNT Thin Film Electrodes

SWNT thin films have been used as transparent electrodes in optoelectronic devices such as solar cells [2], organic light emitting diodes [80], photodetectors [81] and electrochromic [82] devices. SWNT thin films were also preferred in flexible electronics because of their outstanding mechanical properties and homogenous network forming abilities [83].

In this thesis, flexible and transparent ZnO photodetectors utilizing SWNT thin films as transparent electrodes were fabricated via all solution based and cost effective methods.

4.2. Experimental Details

4.2.1. Substrate Cleaning

Prior to SWNT thin film deposition, rigid soda-lime silicate glass and flexible polyethylene terephthalate (PET) substrates were cleaned to get rid of organic residues. Both substrates were cleaned according to the procedure mentioned before in the Chapter 2. All chemicals were purchased from Sigma-Aldrich and used without further purification.

4.2.2. SWNT Thin Film Coating

Carbon Solutions, Inc. purified SWNTs were dispersed in deionized water using sodium dodecyl sulfate (SDS) as a dispersant. This dispersion was sonicated using a 20 kHz tip-sonicator and vacuum filtered onto mixed cellulose ester (MCE) membranes as shown schematically in Figure 4.3 (a). Then, MCE membrane with the SWNT thin film was transferred onto glass or PET substrate by compressive loading as shown in Figure 4.3 (b) and dried at 80 ºC for 2 hours. Finally, the membrane was dissolved by acetone and isopropanol washings. SWNT thin films on the substrate were nitric acid (HNO_3, 65%) treated to decrease their sheet resistance.

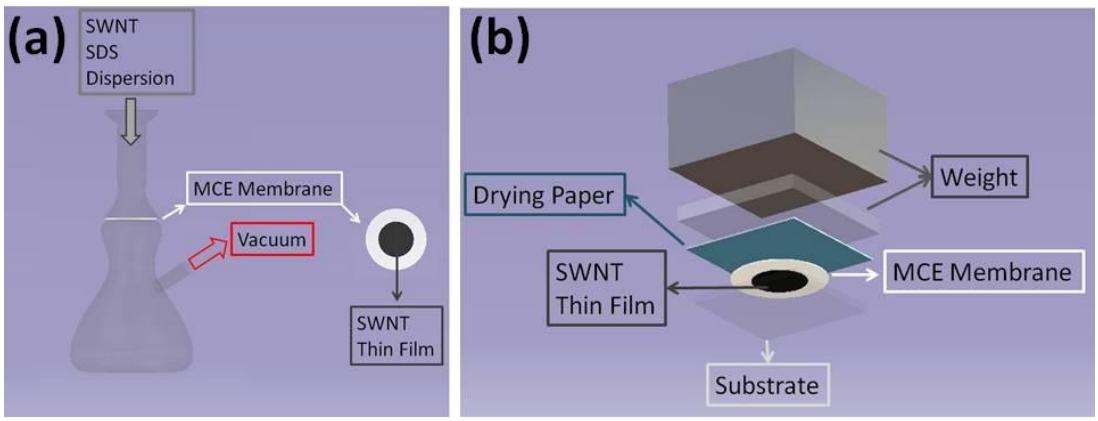

Figure 4.3. Representative schemes of the SWNT thin film deposition process steps.

4.2.3. Hydrothermal ZnO Nanowire Growth

Following the deposition of SWNT thin films, a gap was formed by mechanical means through a razor blade. Size of the gap was measured to be 30 μm. ZnO seed layer was covered on top of the SWNT thin film deposited substrates as described in Chapter 2. In order to investigate the effect of ZnO nanowire density on the

photocurrent, spin coating cycles were repeated for different times. Then, ZnO nanowires were grown by hydrothermal method as described in Chapter 2. Schematic illustration of the fabrication steps are shown in Figure 4.4.

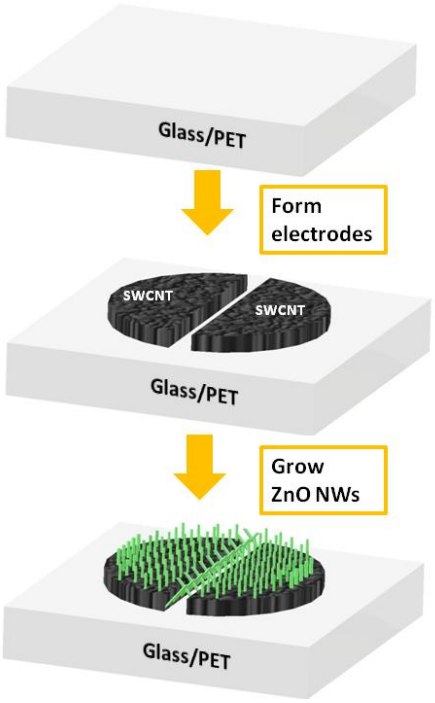

Figure 4.4. Schematic illustration of the fabrication steps of the ZnO nanowire photodetectors.

4.3. Photodetector Characterization Methods

4.3.1. Scanning Electron Microscopy (SEM)

The morphology and the density of the ZnO nanowires were analyzed by FE-SEM (Nova NanoSEM 430) operated at 10 kV. Both top and cross-sectional views of the

SEM images were examined to calculate the nanowire density. Gold coating was used to provide conductivity to substrates for analysis.

4.3.2. Transparency Measurements

The transparency analysis of the SWNT thin films and the devices with different ZnO nanowire densities were done by UV-VIS spectroscopy (Varian-Cary100 Bio). 300 to 800 nm wavelength range was scanned at room temperature in normal incidence mode. Plain substrate backgrounds have been subtracted from the spectra.

4.3.3. Spectral Response Measurements

The spectral response measurement of the ZnO nanowire photodetectors were carried out at room temperature using the spectral response set-up schematically shown in Figure 4.5. The radiated light was generated by Newport Oriel Apex Monochromator Illuminator with a halogen lamp light source. The beam of light was directed into a Newport Oriel 74125 Monochromator. The resulting monochromatic light having within the range of wavelengths from 300 to 800 nm was projected on the ZnO nanowire photodetectors through the quartz optical window of the cryostat. A bias voltage of 2V was applied via a Keithley 2400 sourcemeter. The obtained photoresponse spectrum was corrected for the spectral distribution of the illumination light. The power spectrum of the light radiated by the Newport Oriel Apex Monochromator Illuminator halogen lamp was obtained by means of a Newport powermeter.

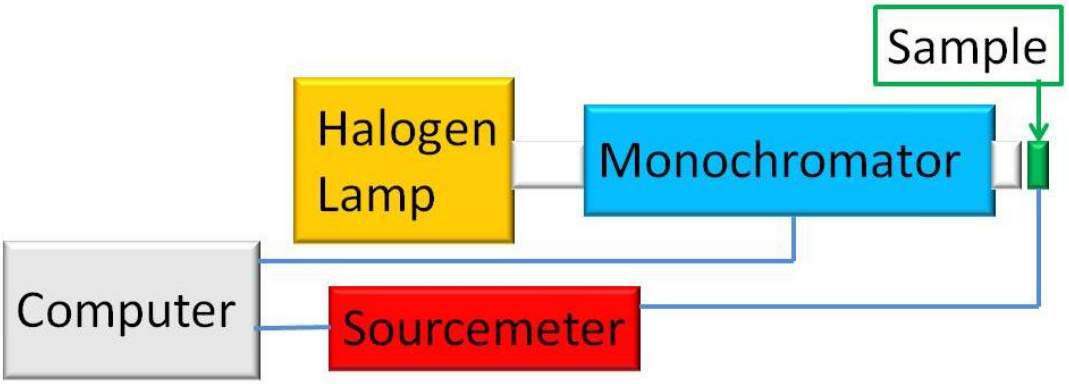

Figure 4.5. The schematic diagram of the spectral response measurement set-up.

4.3.4. Current-Voltage Measurements

Current-voltage measurements have been made using a Keithley 2400 sourcemeter as the voltage source. Voltage was swept between -2 V to 2 V for all samples using a Labview program. Silver dag is used for connections.

4.3.5. Photocurrent Measurements

Photocurrent measurements were made under a constant DC bias of 2 V applied by a Keithley 2400 sourcemeter. Photocurrents under dark and UV illumination were recorded by switching the UV lamp on and off.

4.4. Results

4.4.1. Characterization of the Rigid Device

4.4.1.1. Determination of Nanowire Morphology and Density

It was know that the spin coating cycles control the density of ZnO nanowire. In order to investigate the effect of ZnO nanowire density on the photocurrent, seed solution was spin coated for different times. Figure 4.6 shows the SEM images of ZnO nanowires grown in between the gap of SWNT thin film electrodes. It can be clearly seen from Figure 4.6 that the ZnO nanowires were grown seldomly for the sample spin coated for one time. Nanowire density was calculated to be 1 NW/μm^2 for this sample. It was observed that more and more nanowires were grown and filled the gap in between the SWNT electrodes as the number of spin coating cycles was increased. Nanowire densities were calculated to be 30, 70 and 100 NW/ μm^2 corresponding to spin coating times of 3, 5 and 10 times, respectively. For further investigation of the device structure, cross-sectional SEM images were obtained by cleaving the samples. Top-view and cross-sectional SEM images of the device that have a nanowire density of 100 NW/ μm^2 were shown in Figure 4.7. Red colored SWNT bundles can be clearly seen below the ZnO nanowires.

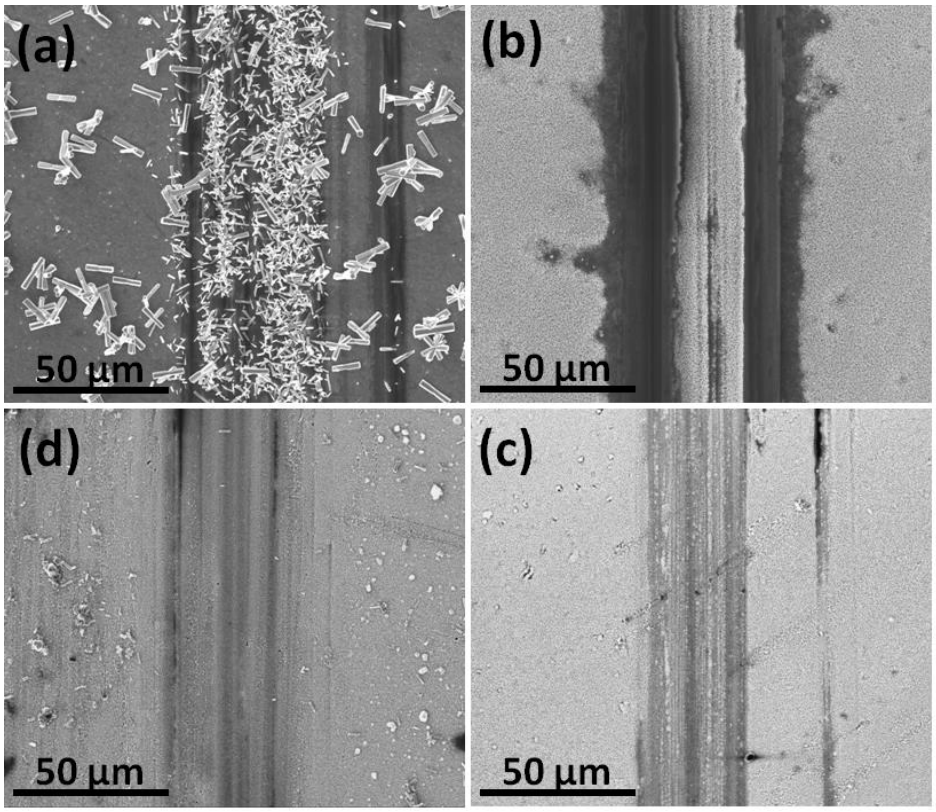

Figure 4.6. Top-view SEM images of the ZnO nanowires grown in between the gap of SWNT thin film electrodes as a result of (a) 1, (b) 30, (c) 70 and (d) 100 NW/µm^2.

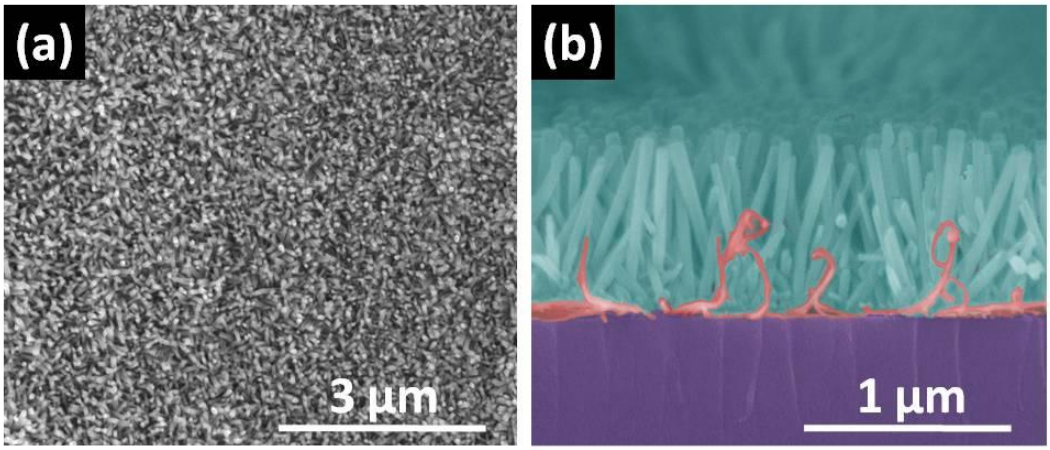

Figure 4.7. (a) Top-view and (b) false colored cross-sectional SEM images of the ZnO nanowires grown in between the gap of SWNT thin film electrodes.

4.4.1.2. Effect of Nanowire Density on Transparency

To investigate the effect of nanowire density on device transparency, transmittance spectra for four different devices were obtained and shown in Figure 4.8. Transmittance of the bare SWNT thin film was also provided for comparison. Lowest transmittance value was found to be 69% at 550 nm for the device that have a nanowire density of 100 NW/μm^2. However, even behind this sample, METU logo was seen clearly in Figure 4.8 (b). Transmittance of the bare SWNT thin film was found to be 88% and decreased to 82%, 81% and 71% at 550 nm for the devices that have nanowire densities of 1, 30 and 70 NW/ μm^2, respectively. This decrease in the transmittance can be explained by the increased amount of light scattering with the increased nanowire density. Photographs of these devices (Figure 4.8 (b)) reveal that although nanowire density decreases the transmittance values, ZnO nanowire photodetectors can be still fabricated with sufficient transparency.

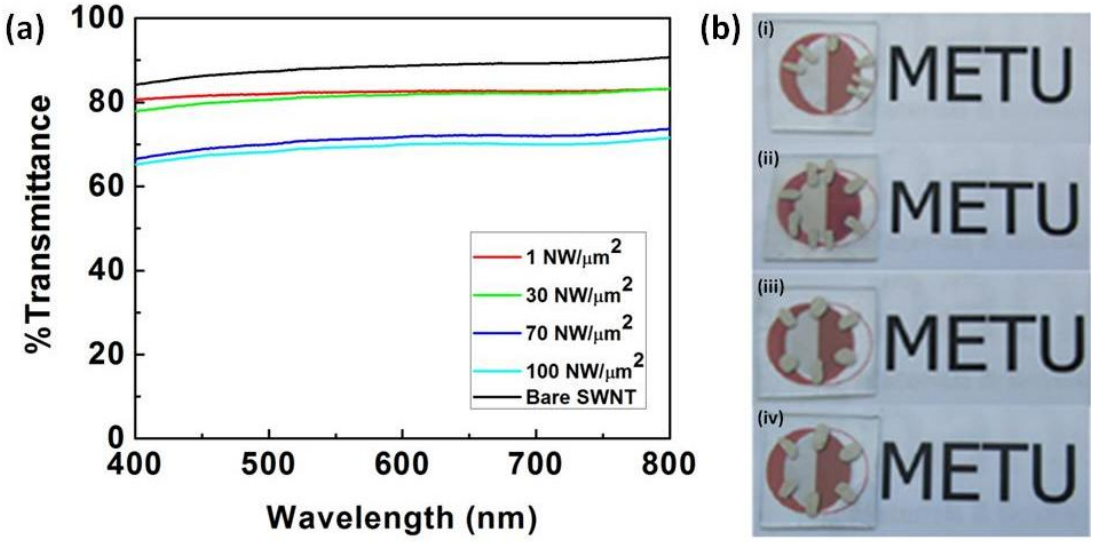

Figure 4.8. (a) Transmittance spectra of the ZnO photodetectors with different nanowire densities. (b) Photographs of the fabricated and measured ZnO photodetectors with nanowire densities of (a) 1, (b) 30, (c) 70 and (d) 100 NW/ μm^2.

4.4.1.3. Spectral Response Measurements

Semiconductors, in our case ZnO, can absorb photons with energies above their bandgap. Using this fact spectral response, which is the ratio of the current generated by the photodetector to the power of the incident light on the photodetector, measurements in a wavelength range of 300 to 800 nm was conducted. Spectral response of the ZnO nanowire photodetector that have a nanowire density of 100 NW/μm^2 at a forward bias of 2 V is shown in Figure 4.9. Responsivity only in the UV range, which has higher energies than 3.37 eV, and a sharp cutoff above 380 nm, was observed. In Chapter 3, PL measurements of the ZnO nanowires were revealed that the near band edge absorption of ZnO is about 380 nm indicating the rationality of the obtained result.

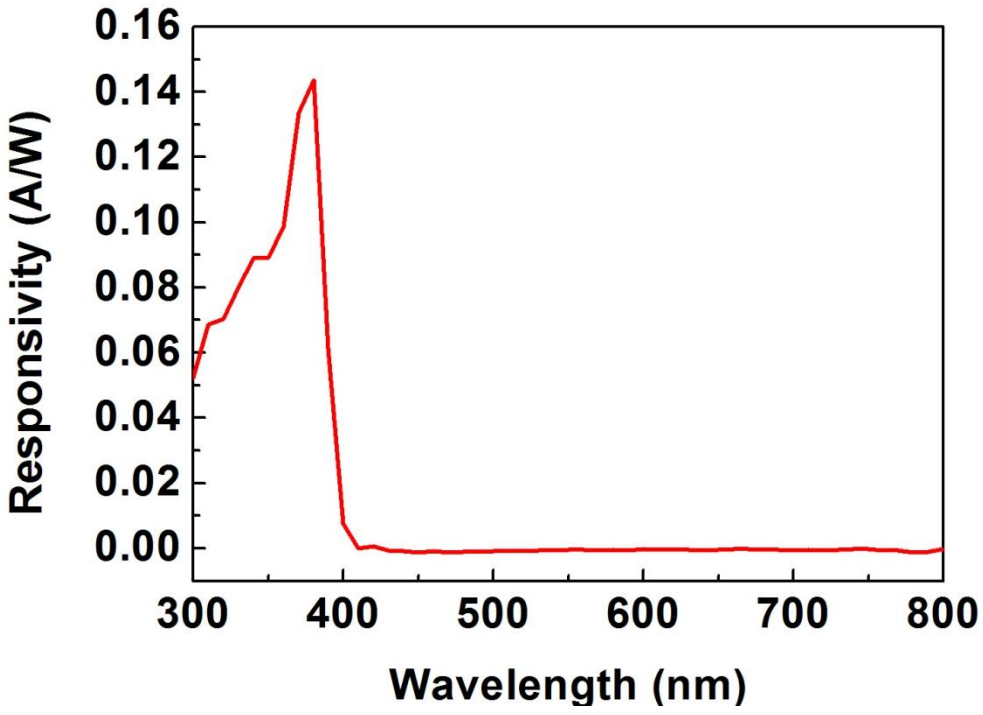

Figure 4.9. Spectral response of the fabricated ZnO nanowire photodetector.

4.4.1.4. Current-Voltage Characteristics

Current-voltage characteristics of all four devices was measured and observed that they reveal very similar device characteristics as shown in Figure 4.10. The measured current increased with the voltage and it is symmetric and quasi-linear. These results reveal that instead of ohmic nanowire-electrode junction, highly resistant nanowire-nanowire junctions dominated conduction. Under an applied bias of 2V, dark currents were measured to be 0.11, 0.11, 0.43, 0.5 μA for the devices with nanowire densities of 1, 30, 70 and 100 NW/ μm^2, respectively. Under UV illumination photons with energies higher than the bandgap of ZnO got absorbed and generated electron-hole pairs contributing to the photocurrent. Therefore, currents under UV illumination were much higher than the ones under dark and found to be 1.23, 3.58, 11.78 and 141 μA for the devices with nanowire densities of 1, 30, 70 and 100 NW/μm^2, respectively.

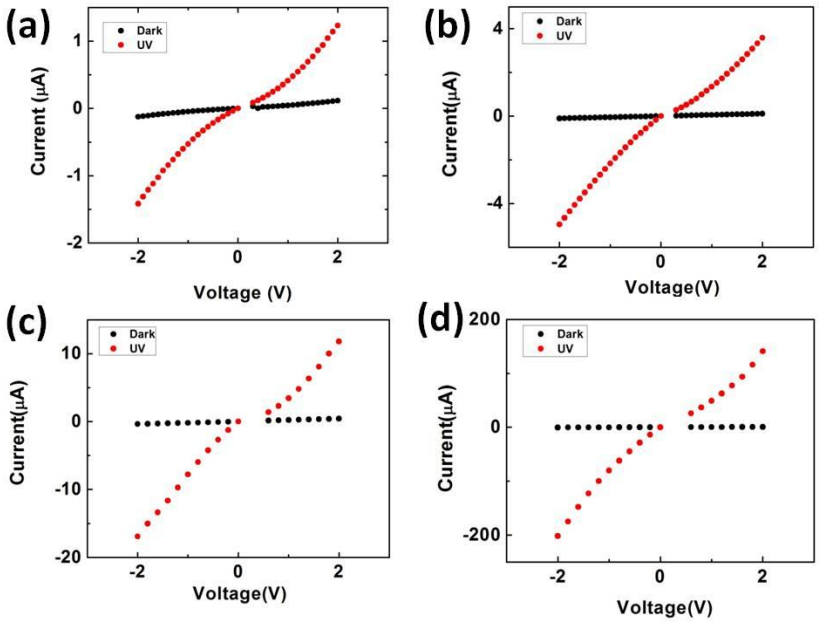

Figure 4.10. Current voltage characteristics of the ZnO nanowire photodetectors with nanowire densities of (a) 1, (b) 30, (c) 70 and (d) 100 NW/μm^2.

4.4.1.5. Photocurrent Measurements

Firstly, photocurrent measurements were done under UV illumination to investigate the saturation time and maximum photoresponse current. Figure 4.11 shows the change in the maximum response currents according to the nanowire density at an applied bias voltage of 2 V. Maximum photoresponse currents were found to be in proportion with the nanowire density.

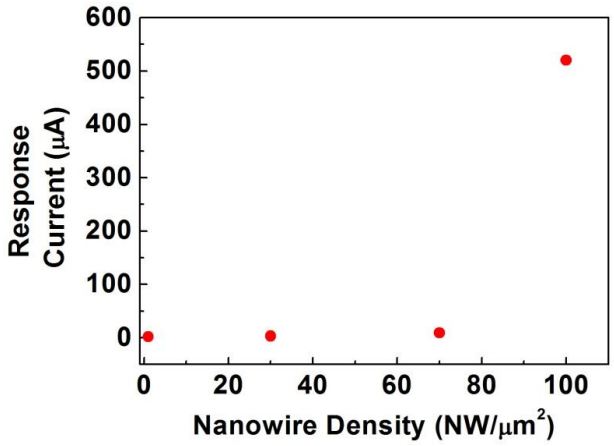

Figure 4.11. Maximum photoresponse currents with nanowire density.

Following the investigation of saturation characteristics, photoresponse current measurements were conducted by switching the UV lamp on and off. Variations of the photoresponse current with time at an applied bias of 2 V for those four devices are shown in Figure 4.12. As a result of the proportionality with nanowire density, the device that has a nanowire density of 100 NW/μm^2 seems to overpower the others.

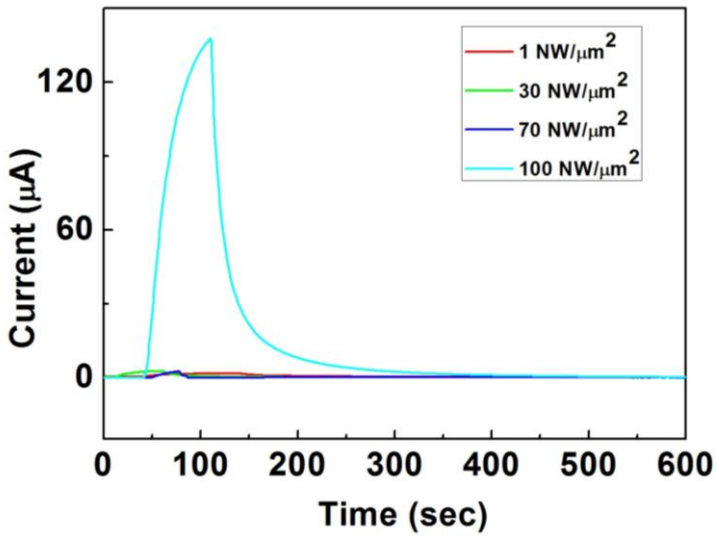

Figure 4.12. Photoresponse of the ZnO photodetectors with different nanowire densities under UV irradiance and a bias voltage of 2 V.

Under an applied bias of 2 V, the dark current and photocurrent of the device with a nanowire density of 100 NW/μm^2 was measured to be 2x10^{-9} and 5.2x10^{-4} A, respectively, yielding an on/off current ratio of 260000, which is far better when compared to the values reported in literature [21, 87]. The recovery time (τ) is defined as the time it takes the photocurrent to fall from its steady-state value to a value that is 36.8% of its the steady-state value. In order to investigate the photoresponse characteristics of the samples, recovery times were calculated. The recovery time for the device with a nanowire density of 100 NW/μm^2, as shown in Figure 4.13 was found to be 16 seconds. This is much more faster than the recovery time of the device with a nanowire density of 1 NW/μm^2 (about 56 seconds) and nearly the same with the photodetectors fabricated with ZnO nanowires produced with similar methods [17, 84]. It was revealed that the oxygen adsorption and desorption controls the photoresponse process [85]. Figure 4.14 (a) schematically represents the dark conditions. Under dark conditions, oxygen molecules adsorbed on the surface of ZnO nanowires, trap free electrons of the n-type semiconductor [$O_2+e^- \rightarrow O_{2(ad)}^-$]. This decreases the carrier density in the nanowires and the

mobility of remaining electrons by creating depletion layers near the surface. Due to their large surface-to-volume ratio, the adsorption of O_2 significantly decreases the conductivity of the nanowires. Upon UV illumination, which is schematically represented in Figure 4.14 (b), electron and hole pairs are generated [$hV \rightarrow e^- + h^+$]. These photocarriers immediately increase the conductivity due to the sudden increase in the nanowire carrier density. Holes migrate to the surface and recombine with the oxygen trapped electrons and release the O_2^- from the surface [$O_{2\,(ad)}^- + h^+ \rightarrow O_{2\,(g)}$]. The remaining unpaired electrons became major carriers and contribute to the current until they are trapped again by readsorbed O_2 on the surface. Photocurrent rises gradually during UV illumination until desorption and readsorption of O_2 reach an equilibrium state. After turning off the UV illumination, holes recombine with electrons; however, there are still a lot of electrons remaining in the nanowires. The reason for this is that at the end of the illumination, the hole density is much lower than the electron density in the nanowires. O_2 molecules readsorb on the surface and trap the remaining unpaired electrons as shown in Figure 4.14 (c). As a result of the large number of these unpaired electrons, current decay becomes slower and recovery time gets longer.

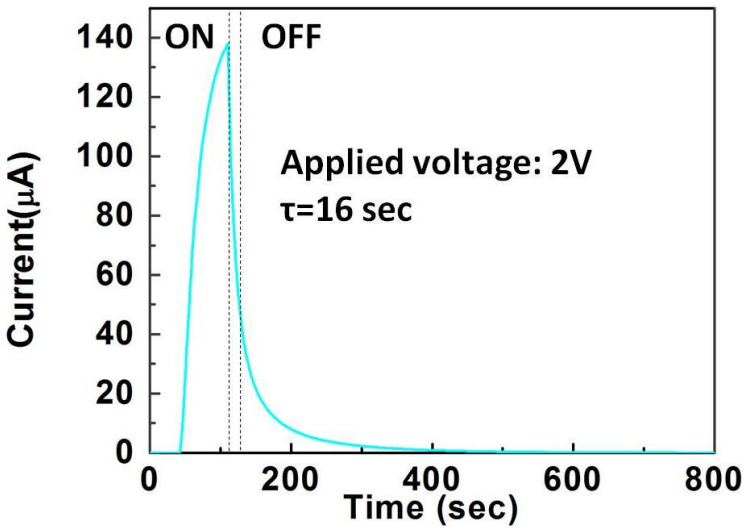

Figure 4.13. Response and recovery current curve of the device that has a nanowire density of 100 NW/μm^2 at an applied bias of 2V.

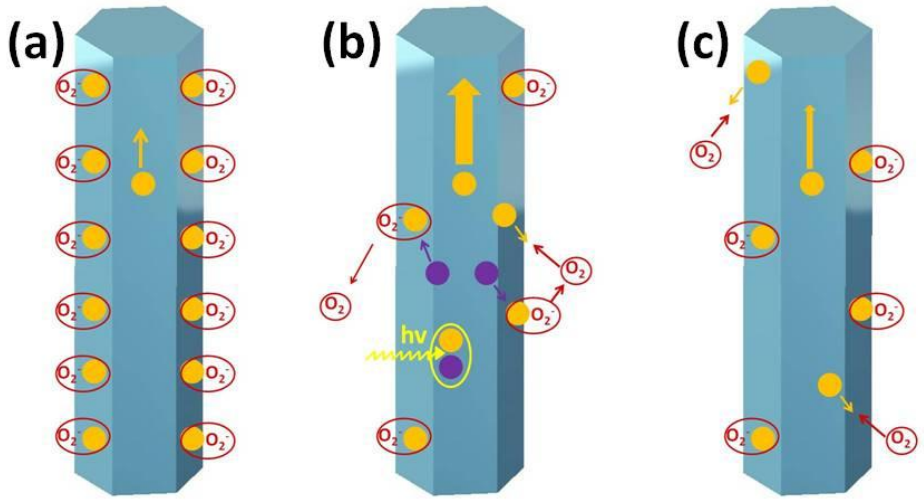

Figure 4.14. Schematic illustration of the photoresponse process. Purple and orange dots are representing holes and electrons, respectively.

4.4.2. Characterization of the Flexible Devices

4.4.2.1. Current-Voltage Characteristics

Current-voltage characteristics of flexible devices fabricated on PET substrate were also measured and shown in Figure 4.15. It has been observed that the flexible devices reveal very similar device characteristic to their rigid counterparts. Figure 4.15 shows that the measured current increases with the voltage and is symmetric and quasi-linear. These results reveal that instead of ohmic nanowire-electrode junction, highly resistant nanowire-nanowire junctions dominated conduction also in flexible devices. Under an applied bias of 2V, dark current and photoresponse current under UV illumination was found to be 0.02 and 8.25 μA, respectively. Photocurrent under UV illumination was found to be higher than the dark current due to the absorbed photons, with energies higher than the bandgap of ZnO, that generate electron-hole pairs contributing to the photocurrent.

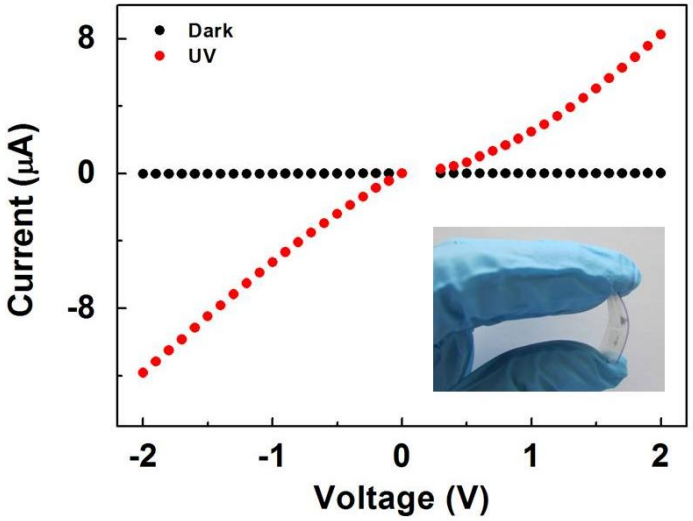

Figure 4.15. Current-voltage characteristics of the fabricated flexible ZnO nanowire photodetector. Inset reveals the photograph of the fabricated flexible ZnO nanowire photodetector.

4.4.2.2. Photocurrent Measurements

To investigate the flexible device performance, photocurrent measurements of the flexible device were performed under strain, while bend to different radius of curvatures. Photograph of the bending set-up and the bended device are shown in Figure 4.16.

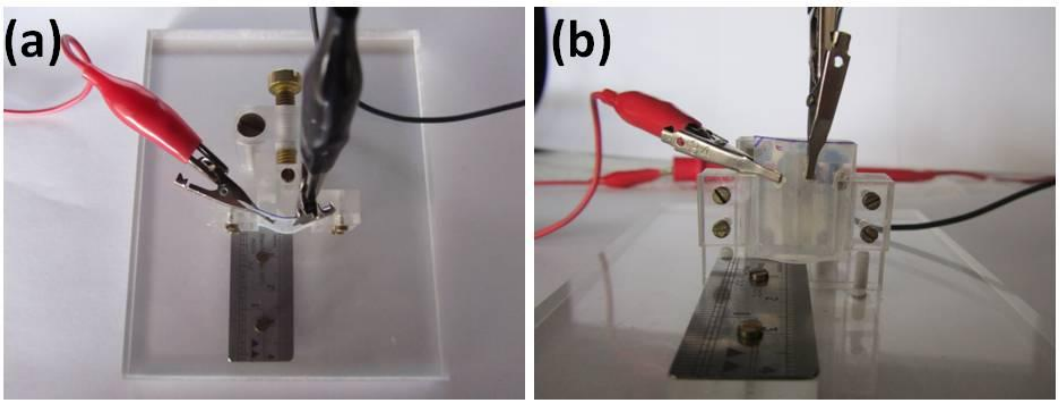

Figure 4.16. Photograph of the bending set-up and the flexible device.

Figure 4.17 shows the variation of the photoresponse current while bent to different radius of curvatures at an applied bias of 2 V. It was observed that the performance of the device stay nearly unchanged. Photocurrent was found to increase when the radius of curvature of the substrate was increased. This situation can be attributed to the improved mechanical coupling between the SWNT electrodes and ZnO nanowires.

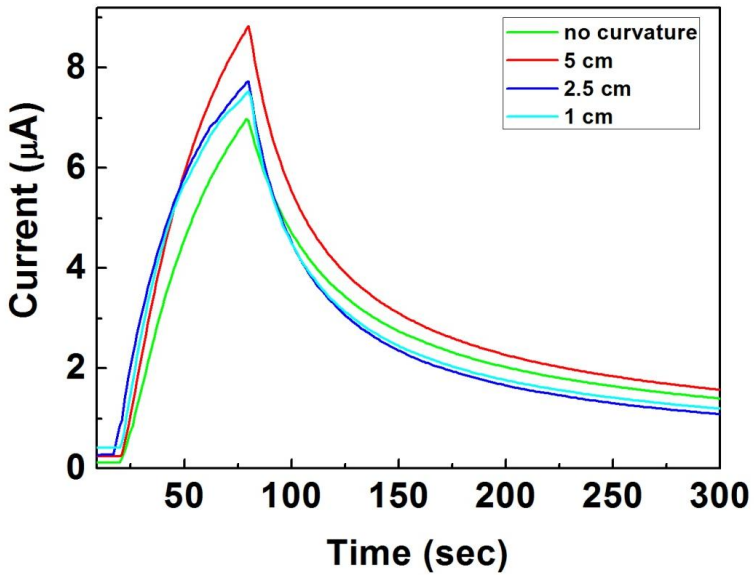

Figure 4.17. Response and recovery current characteristics of the fabricated flexible ZnO nanowire photodetectors under strain.

CHAPTER 5

CONCLUSIONS AND FUTURE RECOMMENDATIONS

5.1. Conclusions

In this thesis, utilization of hydrothermally grown ZnO nanowires in hybrid LEDs and photodetectors was investigated.

In the first part, hybrid LED structures were fabricated utilizing complementary ZnO nanowires and p-type semiconducting polymers. Cost-effective fabrication methods were chosen to fabricate hybrid LED structures. At the first stage of the fabrication, ZnO nanowire arrays were hydrothermally grown; then at the second stage, hybrid structures were formed by spin coating of different hole conducting polymers. Current-voltage characterizations of the fabricated devices revealed the rectifying behavior of the hybrid LED structures. Ideality factors were found to be larger than the ideal ones. This non-ideal behavior of the devices was attributed to the defect states in ZnO nanowires, which is further investigated by the photoluminescence measurements. Photoluminescence measurements revealed the emission wavelengths of NBE and DLE emissions of ZnO and excitonic emission of the semiconducting polymers. Using this data, electroluminescence results were examined. The UV emission peaks and the broader peaks that were observed during the electroluminescence measurements of the hybrid LEDs were attributed to the NBE emissions of ZnO and combination of the main emission peak of polymer and DLE emissions of ZnO, respectively.

In the second part, flexible and transparent UV photodetectors were fabricated utilizing ZnO nanowires. Again, all solution based and cost-effective methods were used to fabricate the photodetectors. SWNT thin films were used as electrodes. Following the deposition of SWNT thin film electrodes by vacuum filtration, ZnO nanowires were synthesized through hydrothermal method. Effects of ZnO nanowire density on the optoelectronic properties of the fabricated devices were investigated. Transmittance of the fabricated devices was found to be varying between 69%-88%. Spectral response measurements revealed that the devices were only responsive to UV range. Decay time was calculated to be 16 seconds, which is comparable to the values reported in literature. Moreover, on/off current ratio was calculated to be 260000. Photoresponse current measurements of the flexible devices were also examined under strain while bend to different radius of curvatures. The results revealed that the photoresponse current was increased with the radius of curvature due to the improved mechanical coupling between the SWNT electrodes and ZnO nanowires.

5.2. Future Recommendations

In this thesis, hydrothermally grown ZnO nanowires were used as electrically active components in LEDs and UV photodetectors. MEH-PPV and PFO used as hole conducting polymer in hybrid LEDs. Power efficiencies of the light emissions could not be measured with the available powermeter. Powermeter may be modified to detect the emission or different hole conducting polymers can be investigated to improve the emission intensity.

On the other hand, ZnO nanowires were grown vertically in between the gap of SWNT thin film electrodes to fabricate UV photodetectors and the electrical conduction was provided through the mechanical coupling between the SWNT electrodes and ZnO nanowires. Electrical conductivity can be improved; thus, the response time can be further decreased by the growth of ZnO nanowires horizontally between the two electrodes.

REFERENCES

[1] International Energy Agency, 2006, "Light` s Labour` s Lost," IEA Publications.

[2] Unalan H. E., 2008, "Flexible Organic Photovoltaics from Zinc Oxide Nanowires Grown on Transparent and Conducting Single Walled Carbon Nanotube Thin Film," Journal of Materials Chemistry, **18**, pp. 5909–5912.

[3] Lim Z.H., Chia Z.X., Kevin M., Wong A. S.W., and Ho G.W., 2010, "A Facile Approach Towards ZnO Nanorods Conductive Textile for Room Temperature Multifunctional Sensors," Sensors and Actuators B: Chemical **151**, pp. 121-126.

[4] Soci C., Zhang A., Xiang B., Dayeh S. A., Aplin D.P.R., Park J., Bao X.Y., Lo Y.H., and Wang D., 2007, "ZnO Nanowire UV Photodetectors with High Internal Gain," Nano Letters **7**, pp. 1003-1009.

[5] Könenkamp R., Word R.C., and Schlegel C., 2004, "Vertical Nanowire Light-Emitting Diode," Applied Physics Letters **85**, pp. 6004-6006.

[6] Wei S.H., Li J., and Yan Y. 2008, "Design of Shallow p-type Dopants in ZnO," 33rd IEEE Photovoltaic Specialist Conference, California.

[7] Sellappan R., 2008, "Light Emitting Diodes Based on n-type ZnO Nanorods and p-type Organic Semiconductors," MS Thesis Linköping University, pp. 9.

[8] Park W., and Yi G.C., 2004, "Electroluminescence in n-ZnO Nanorod Arrays Vertically Grown on p-GaN," Advanced Materials, **16**, pp. 87-90.

[9] Lupan O., Pauporte T., and Viana B., 2010, "Low-Voltage UV-Electroluminescence from ZnO-Nanowire Array/p-GaN Light-Emitting Diodes," Advanced Materials, **22**, pp. 3298-3302.

[10] Kim D.C., Han W. S., Cho H.K., Kong B.H., and Kim H.S., 2007, "Multidimensional ZnO Light-Emitting Diode Structures Grown by Metal Organic Chemical Vapor Deposition on p-Si," Applied Physics Letters, **91**, pp. 231901-231903.

[11] Hsieh Y.P., Chen H.Y., Lin M. Z., Shiu S. C., Hofmann M. C., Ming Y. J., Xiaoting Y., Ying J., Chang H.J., Huang H.M., Tseng, S.C., Chen L.C., Chen K.H.,

Lin C.F., Liang C.T., Chen Y.F., 2009, "Electroluminescence from ZnO/Si Nanotips Light Emitting Diodes," Nanoletters, **9**, pp. 1839-1843.

[12] Sun H., Zhang Q.F., Wu J.L., 2006, "Electroluminescence from ZnO Nanorods with an n-ZnO/p-Si Heterojunction Structure," Nanotechnology, **17**, pp. 2271–2274.

[13] Könenkamp R., Word A.R.C., Dosmailov M., Meiss J., and Nadarajah A., 2007, "Selective Growth of Single-Crystalline ZnO Nanowires on Doped Silicon," Journal of Applied Physics, **102**, pp. 56103- 56105.

[14] Zainelabdin A., Zaman S., Amin G., Nur O., Willander M., 2010, "Stable White Light Electroluminescence from Highly Flexible Polymer / ZnO Nanorods Hybrid Heterojunction Grown at 50 ° C," Nanoscale Research Letters, **5**, pp. 1442–1448.

[15] Black H. S., 2004, "ROS: a step closer to elucidating their role in the etiology of light-induced skin disorders," Journal of Investigative Dermatology, **122**, pp. 13-14.

[16] Liebler D.C., 2006, "The poisons within: application of toxicity mechanisms to fundamental disease processes," Chemical Research in Toxicology **19**, pp. 610-613.

[17] Zhou H., Fang G., Liu N., Zhao X., 2011, "Ultraviolet photodetectors based on ZnO nanorods-seed layer effect and metal oxide modifying layer effect," Nanoscale Research Letters, **6**, pp. 147-152.

[18] Hsu C.L., Chang, S.J., Lin Y.R., Li P.C., Lin T.S., Tsai S.Y., 2005, "Ultraviolet photodetectors with low temperature synthesized vertical ZnO nanowires," Chemical Physics Letters, **416**, pp. 75-78.

[19] Chang S.P., Chien Y.L., Chang S.J., Chiou Y.Z., Hsueh T.J., and Hsu C.L., 2011, "Electrical and Optical Characteristics of UV Photodetector With Interlaced ZnO Nanowires," IEEE Journal of Selected Topics in Quantum Electronics, **17**, pp. 990-995.

[20] JinY., Wang J., Sun B., Blakesley J.C., Greenham N.C., 2008, "Solution-processed ultraviolet photodetectors based on colloidal ZnO nanoparticles," Nano Letters, **8**, pp. 1649-1653.

[21] Jung B. O., Kim D. C., Kong B. H., Kim D.W., Cho H. K., 2011, "Fully transparent vertically aligned ZnO nanostructure-based ultraviolet photodetectors with high responsivity," Sensors and Actuators B: Chemical, **160**, pp. 740-746.

[22] Lin Y. H., Lee P.S., Hsueh Y. C., Pan K.Y., Kei C.C., Chan M.H., Wu J.M., Perng T. P., Shih H.C., 2011, "Atomic Layer Deposition of Zinc Oxide on Multiwalled Carbon Nanotubes for UV Photodetector Applications," Journal of The Electrochemical Society, **158**, pp. 24-27.

[23] Cao G., 2004, “Nanostructures and Nanomaterials,” Imperial College Press.

[24] Taniguchi N., 1974, “On the Basic Concept of 'Nano-Technology'” Proceedings of the International Conference on Production Engineering, Part II, Japan Society of Precision Engineering.

[25] Drexler K.E., 1981, “Molecular engineering: An approach to the development of general capabilities for molecular manipulation,” Proceedings of the National Academy of Sciences, **78**, pp. 5275-5278.

[26] Roduner E., 2006, “Size matters: why nanomaterials are different,” Chemical Society Reviews, **35**, pp. 583–592.

[27] Ashby M.F., Ferreira P.J., Schodek D.L., 2009, “Nanomaterials Nanotechnologies and Design,” Elsevier.

[28] Bhushan B., 2004 “Springer Handbook of Nanotechnology,” Springer.

[29] Kum M.C.M., 2009 “Fabrication, Device Assembly, and Application of One-Dimensional Chalcogenides Nanostructures,” PHD thesis University of California Riverside, pp. 1.

[30] Coleman V. A., Bradby J. E., Jagadish C., Munroe P., Heo Y. W., Pearton S. J., Norton D. P., Inoue M., Yano M., 2005, “Mechanical properties of ZnO epitaxial layers grown on a- and c-axis sapphire,” Applid Physics Letters, **86**, pp. 203105.

[31] Zhao Q.X., Klason P., Willander M., 2007, “Growth of ZnO nanostructures by vapor–liquid–solid method,” Applied Physics A, **88**, pp. 27-30.

[32] Lee W., Jeong M.C., Myoung J.M., 2004, “Fabrication and application potential of ZnO nanowires grown on GaAs(002) substrates by metal–organic chemical vapour deposition,” Nanotechnology, **15**, pp. 254-259.

[33] Wadeasa A., Nur O., Willander M., 2009, “The effect of the interlayer design on the electroluminescence and electrical properties of n-ZnO nanorod/p-type blended polymer hybrid light emitting diodes,” Nanotechnology, **20**, pp. 65710-65715.

[34] Son H.J., 2007, “Synthesis of ZnO nanowires by pulsed laser deposition in furnace,” Applied Surface Science, **253**, pp. 7848–7850.

[35] Tiwari J. N., Tiwari R. N., Kim K.S., 2012, “Zero-dimensional, one-dimensional, two-dimensional and three-dimensional nanostructured materials for advanced electrochemical energy devices,” Progress in Materials Science, **57**, 724-803.

[36] Anthony S.P., Lee J.I., Kim J.K., 2007, "Tuning optical bandgap of vertically aligned ZnO nanowire arrays grown by homoepitaxial electrodeposition," Applied Physics Letters, **90**, 103107-103110.

[37] Pan C.J., Chen C.W., Chen J.Y., Huang P.J., Chi G.C., Chang C.Y., Ren F., Pearton S.J., 2009, "Optical and structural properties of Eu-diffused and doped ZnO nanowires," Applied Surface Science, **256**, pp. 187-190.

[38] Xu L., Guo Y., Liao Q., Zhang J., Xu D., 2005, "Morphological Control of ZnO Nanostructures by Electrodeposition," The Journal of Physical Chemistry. B, **109**, pp. 13519-13522.

[39] Byrappa K., Yoshimura M., 2001, "Handbook of Hydrothermal Technology," Noyes Publications.

[40] Li Q., Kumar V., Li Y., Zhang H., Marks T.J., Chang, R. P. H., 2005, "Fabrication of ZnO Nanorods and Nanotubes in Aqueous Solutions," Chemistry of Materials, **17**, 1001-1006.

[41] Akgun M.C., 2012, "A Parametric Study On Hydrothermal Synthesis Of Zinc Oxide Nanowires With Various Zinc Salts," MS Thesis Middle East Technical University.

[42] Stern, N., 2006, "Stern Review: The Economics of Climate change," HM Treasury.

[43] U.S. Department of Energy, 2009, "2009 Building Energy Data Book" http://buildingsdatabook.eren.doe.gov/ (Last visited on 30.05.2012).

[44] Zukauskas A., Vaicekauskas R., Ivanauskas F., Vaitkevicius H., and Shur M.S., 2008, "Spectral Optimization of Phosphor Conversion Light Emitting Diodes for Ultimate Color Rendering," Applied Physics Letters, **93**, pp. 51115-51118.

[45] Round H.J., 1097, "A Note on Carborundum," Electrical World, **49**, pp. 309.

[46] Violin E.E., Kalnin A.A., Paynkov V.V., Tairov Y.M., Yaskov D.A., 1969, " Silicon Carbide-1986," Materials Research Bulletin, pp. 231.

[47] Nathan M.I., Dumke W.P., Burns G., Dill F.H., and Lasher G., 1962 "Stimulated Emission of Radiation From GaAs p-n Junctions," Applied Physics Letters, **1**, pp. 62-64.

[48] Quist T. M., Rediker R. H., Keyes R. J., Krag W. E., Lax B., McWhorter A. L., and Zeigler H. J., 1962 "Semiconductor Maser of GaAs," Applied Physics Letters, **1**, pp. 91-92.

[49] Holoyank Jr. N., Bevacqua S.F., 1962, "Coherent Light Emission from $Ga(As_{1-x}P_x)$ Junctions," Applied Physics Letters, **1**, pp. 82-83.

[50] Schubert E.F., 2003, "Light-Emitting Diodes," Cambridge University Press.

[51] Duke C.B. Holoyank Jr. N., 1973, "Advances in Light-Emitting Diodes," Physics Today, **26**, pp. 23.

[52] Pankove J. I., and Lampert M. A., 1974, "Model for Electroluminescence in GaN," Physical Review Letters, **33**, pp. 361–365.

[53] Burroughes J. H., Bradley D. D. C., Brown A. R., Marks R. N., Mackay K., Friend R. H., Burns P. L., Holmes A. B., 1990, "Light-Emitting Diodes Based On Conjugated Polymers," Nature, **347**, 539-541.

[54] Hussain I., Bano N., Hussain S., Nur O., Willander M., 2011, "Study of intrinsic white light emission and its components from ZnO-nanorods / p-polymer hybrid junctions grown on glass substrates," Journal of Materials Science, **46**, 7437-7442.

[55] Sun J., Pal B.N., Jung B. J., Katz H.E., 2009, "Solution-processed hybrid p – n junction vertical diode," Organic Electronics, **10**, pp. 1-7.

[56] Willander M., Nur O., Sadaf J. R., Qadir M. I., Zaman S., Zainelabdin A., Bano N., Hussain I., 2010, " Luminescence from Zinc Oxide Nanostructures and Polymers and their Hybrid Devices," Materials, **3**, pp. 2643-2667.

[57] Wadeasa A., Nur O., Willander M., 2009, "The effect of the interlayer design on the electroluminescence and electrical properties of n-ZnO nanorod/p-type blended polymer hybrid light emitting diodes," Nanotechnology, **20**, pp. 65710-65715.

[58] Hang C.C., 2005, "Fabrication and Characterization of Microcavity Organic Light Emitting Diodes," MP Thesis The University Of Hong Kong.

[59] Winsey S.L., Haldar N.A., Marsh H.P., Bunce M., Marshall S.E., Harris A. L., Wojnarowska F., and Welsh K. I.,2000, "A Variant within the DNA Repair Gene XRCC3 Is Associated with the Development of Melanoma Skin Cancer," Cancer Research, **60**, pp. 5612–5616.

[60] World Health Organization, "Ultraviolet Radiation," http://www.who.int/uv/en/ (Last visited on 30.05.2012).

[61] Decoster D., Harari J., 2009 “Optoelectronic Sensors,” John Wiley & Sons, Inc.

[62] Soehnge H., Ouhtit A., Ananthaswamy H.N., 1997, “Mechanisms of Induction of Skin Cancer By UV Radiation,” Frontiers in Bioscience, **2**, pp. 538-551.

[63] Monroy E., Omnes F., Calle F., 2003, “Wide-bandgap semiconductor ultraviolet photodetectors,” Semiconductor Science and Technology, **18**, pp. 33-51.

[64] Liu K., Sakurai M., Aono M., 2010, “ZnO Based Ultraviolet Photodetectors,” Sensors, **10**, pp. 8604-8634.

[65] Liu Y., Gorla C.R., Liang, S., Emanetoglu, N., Lu, Y., Shen, H., Wraback, M., 2000, “Ultraviolet Detectors Based on Epitaxial ZnO Films Grown by MOCVD.,” Journal of Electronic Materials, **29**, pp. 69-74.

[66] Xua Q.A., Zhanga J.W., Juc K.R., Yanga X.D., Houa X., 2006, “ZnO Thin Film Photoconductive Ultraviolet Detector with Fast Photoresponse,” Journal of Crystal Growth, **289**, pp 44-47.

[67] Liu K.W., Ma J.G., Zhang J.Y., Lu Y.M., Jiang D.Y., Li B.H., Zhao D.X., Zhang Z.Z., Yao B., Shen D.Z., 2007, “Ultraviolet Photoconductive Detector with High Visible Rejection and Fast Photoresponse Based on ZnO Thin Film,” Solid State Electronics, **51**, pp. 757-761.

[68] Bi Z., Yang X., Zhang J., Bian X., Wang D., Zhang X., Hou X., 2009, “A back-illuminated Vertical-Structure Ultraviolet Photodetector Based on an RF-Sputtered ZnO Film,” Journal of Electronic Materials, **38**, pp. 609-612.

[69] Liang S., Sheng H., Liu Y., Huo Z., Lu Y., Shen H., 2001, “ZnO Schottky Ultraviolet Photodetectors,” Journal of Crystal Growth 2001, **225**, pp. 110-113.

[70] Li M.Y., Anderson W., Chokshi N., Deleon R.L., Tompa G., 2006, “Laser Annealing of Laser Assisted Molecular Beam Deposited ZnO Thin Films with Application to Metal-Semiconductor-Metal Photodetectors,” Journal of Applied Physics, **100**, pp. 53106-53109.

[71] Li M.Y., Chokshi N., Deleon R.L., Tompa, G., Anderson W.A., 2007, “Radio Frequency Sputtered Zinc Oxide Thin Films with Application to Metal-Semiconductor-Metal Photodetectors,” Thin Solid Films, **515**, pp. 7357-7363.

[72] Shan C.X., Zhang J.Y., Yao B., Shen D.Z., Fan X.W., Choy K.L., 2009, “Ultraviolet Photodetector Fabricated from Atomic-Layer-Deposited ZnO Films,” Journal of Vacuum Science and Technology B, **27**, pp.1765-1768.

[73] Lin T.K., Chang S.J., Su Y.K., Huang B.R., Fujita M., Horikoshi Y., 2005, "ZnO MSM Photodetectors with Ru Contact Electrodes," Journal of Crystal Growth, **281**, pp. 513-517.

[74] Alivov Y.I., Özgür Ü., Dogan S., Johnstone D., Avrutin V., Onojima N., Liu C., Xie J., Fan Q., Morkoç H., 2005, "Photoresponse of n-ZnO/p-SiC Heterojunction Diodes Grown by Plasma-Assisted Molecular-Beam Epitaxy," Applied Physics Letters, **86**, pp. 241108-241111.

[75] Jeong I.S., Kim J.H., Lm S., 2003, "Ultraviolet-Enhanced Photodiode Employing n-ZnO/p-Si Structure," Applied Physics Letters, **83**, pp. 2946-2948.

[76] Kind H., Yan H., Messer B., Law M., Yang P., 2002, "Nanowire Ultraviolet Photodetectors and Optical Switches," Advanced Materials, **14**, pp. 158-160.

[77] Suehiro J., Nakagawa N., Hidaka S., Ueda M., Imasaka K., Higashihata M., Okad, T., Hara M., 2006, "Dielectrophoretic fabrication and characterization of a ZnO nanowire-based UV photosensor," Nanotechnology, **17**, pp. 2567-2573.

[78] Su Y. K., Peng S. M., Ji L. W., Wu C. Z., Cheng W. B., Liu C. H., 2010, "Ultraviolet ZnO nanorod photosensors," Langmuir, **26**, pp. 603-606.

[79] Yingying L., Chuanwei C., Xiang D., Junshan G., Haiqian Z., 2009, "Facile fabrication of UV photodetectors based on ZnO nanorod networks across trenched electrodes," Journal of Semiconductors, **30**, pp. 63004-63007.

[80] Li J., Hu L., Wang L., Zhou Y., Grüner G., and Marks T.J., 2006, "Organic light-emitting diodes having carbon nanotube anodes," Nano Letters, **6**, pp. 2472-2477.

[81] Choi Y., 2010, "Fabrication of Photodetectors using Transparent Carbon Nanotube Films," International Journal of Science and Technology, **24**, pp. 75-82

[82] Hu L., Gruner G., Li D., Kaner R. B., Cech J., 2007, "Patternable transparent carbon nanotube films for electrochromic devices," Journal of Applied Physics, **101**, pp. 16102- 16104.

[83] Sreekumar T.V., Liu T., Kumar S., Ericson L.M., Hauge R.H., Smalley R.E., 2003, "Single-Wall Carbon Nanotube Films," Chemistry of Materials, **15**, pp. 175-178.

[84] Liu N., Fang G., Zeng W., Zhou H., Cheng F., Zheng Q., Yuan L., Zou X., Zhao X., 2010, "Direct Growth of Lateral ZnO Nanorod UV Photodetectors with Schottky Contact by a Single-Step Hydrothermal Reaction," ACS Applied Materials and Interfaces, **2**, pp. 1973-1979.

[85] Li Y.,Della Valle F., Simonnet M., Yamada I., Delaunay J.J., 2009, "Competitive surface effects of oxygen and water on UV photoresponse of ZnO nanowires," Applied Physics Letters, **94**, pp. 23110-23112.

[86] Ozgur U., Alivov Y. I., Liu C., Teke A., Reshchikov M. A., Dogan S., Avrutin V., Cho S.J., Morkoc H., 2005, "A comprehensive review of ZnO materials and devices," Journal of Applied Physics, **98**, pp. 41301-41403.

[87] Bai S., Wu W., Qin Y., Cui N., Bayerl D.J., and Wang X., 2011, "High-Performance Integrated ZnO Nanowire UV Sensors on Rigid and Flexible Substrates," Advanced Functional Materials **21**, pp. 4464-4469.